Neurobiology of Disease 129 (2019) 130–143

Contents lists available at ScienceDirect

Neurobiology of Disease

journal homepage: www.elsevier.com/locate/ynbdi

Altered inhibition and excitation in neocortical circuits in congenital microcephaly

Sami Zaqout[a,b,c,d,1], Kathrin Blaesius[a,b,c,d,1], Yuan-Ju Wu[e], Stefanie Ott[a], Nadine Kraemer[a,b,c], Lena-Luise Becker[a,b,c], Marta Rosário[a], Christian Rosenmund[d,e,f], Ulf Strauss[a,1], Angela M. Kaindl[a,b,c,d,*,1]

[a] Charité – Universitätsmedizin Berlin, Institute of Cell- and Neurobiology, Charitéplatz 1, 10117 Berlin, Germany
[b] Charité – Universitätsmedizin Berlin, Center for Chronically Sick Children (Sozialpädiatrisches Zentrum, SPZ), Augustenburger Platz 1, 13353 Berlin, Germany
[c] Charité – Universitätsmedizin Berlin, Department of Pediatric Neurology, Augustenburger Platz 1, 13353 Berlin, Germany
[d] Berlin Institute of Health (BIH), Anna-Louisa-Karsch Strasse 2, 10178 Berlin, Germany
[e] Charité – Universitätsmedizin Berlin, NeuroCure, Charitéplatz 1, 10117 Berlin, Germany
[f] Charité – Universitätsmedizin Berlin, Institute of Neurophysiology, Charitéplatz 1, 10117 Berlin, Germany

ARTICLE INFO

Keywords:
Cdk5rap2
Microcephaly
Neuronal differentiation
Synaptic transmission
Dendritic morphogenesis

ABSTRACT

Congenital microcephaly is highly associated with intellectual disability. Features of autosomal recessive primary microcephaly subtype 3 (MCPH3) also include hyperactivity and seizures. The disease is caused by biallelic mutations in the Cyclin-dependent kinase 5 regulatory subunit-associated protein 2 gene *CDK5RAP2*. In the mouse, *Cdk5rap2* mutations similar to the human condition result in reduced brain size and a strikingly thin neocortex already at early stages of neurogenesis that persists through adulthood. The microcephaly phenotype in MCPH arises from a neural stem cell proliferation defect. Here, we report a novel role for Cdk5rap2 in the regulation of dendritic development and synaptogenesis of neocortical layer 2/3 pyramidal neurons. Cdk5rap2-deficient murine neurons show poorly branched dendritic arbors and an increased density of immature thin spines and glutamatergic synapses *in vivo*. Moreover, the excitatory drive is enhanced in *ex vivo* brain slice preparations of *Cdk5rap2* mutant mice. Concurrently, we show that pyramidal neurons receive fewer inhibitory inputs. Together, these findings point towards a shift in the excitation – inhibition balance towards excitation in *Cdk5rap2* mutant mice. Thus, MCPH3 is associated not only with a neural progenitor proliferation defect but also with altered function of postmitotic neurons and hence with altered connectivity.

1. Introduction

Autosomal recessive primary microcephaly (MicroCephaly Primary Hereditary; MCPH) is a rare neurodevelopmental disorder characterized by intellectual disability and microcephaly at birth due to severe reduction in brain volume that affects especially the neocortex (Kaindl et al., 2010; Kraemer et al., 2011). So far, twenty five genes have been linked to MCPH and are referred to as MCPH1-25 (DiStasio et al., 2017; Kadir et al., 2016; Moawia et al., 2017; reviewed in Zaqout et al., 2017b). Some MCPH patients have epilepsy and/or a hyperactivity disorder (Passemard et al., 2009). Biallelic mutations in the gene encoding centrosomal Cyclin-dependent kinase 5 regulatory subunit-associated protein 2 (CDK5RAP2) lead to MCPH3 (MIM*604804) (Bond et al., 2005; Hassan et al., 2007; Issa et al., 2013b).

MCPH is seen as model disorder for microcephaly. Thus, unraveling pathomechanisms of this disease can convey insight into basic mechanisms of physiologic brain development, particularly of brain growth and cortex formation. One current model for the microcephaly phenotype in MCPH invokes a premature shift from symmetric to asymmetric cell divisions and thus premature neurogenesis with a subsequent depletion of the progenitor pool (Buchman et al., 2010; Fish et al., 2006; Lizarraga et al., 2010). In addition, increased apoptosis of neural progenitors and postmitotic cells has been reported in MCPH3 mice (Kraemer et al., 2015; Lizarraga et al., 2010). Premature neurogenesis due to CDK5RAP2 dysfunction may be secondary to disturbances in cleavage plane orientation of apical neural progenitors (Lizarraga et al., 2010), altered centriole engagement and cohesion (Barrera et al., 2010), microtubule organizing dysfunction of the

* Corresponding author at: Institute for Cell Biology and Neurobiology, Charité – Universitätsmedizin Berlin, Charitéplatz 1, 10117 Berlin, Germany.
E-mail address: angela.kaindl@charite.de (A.M. Kaindl).
[1] These authors contributed equally to this work.

https://doi.org/10.1016/j.nbd.2019.05.008
Received 18 December 2018; Received in revised form 15 April 2019; Accepted 11 May 2019
Available online 15 May 2019
0969-9961/

centrosome through interaction with the gamma tubulin ring complex (Fong et al., 2008), improper spindle formation and chromosome segregation (Bond et al., 2005). Most studies regarding the pathophysiology of MCPH have focused on division and survival of neural progenitors. The effect of MCPH proteins on neuronal differentiation and function within the neural circuit, however, has been largely neglected. Since a smaller brain does not necessarily imply intellectual disability but MCPH patients often display such condition together with hyperactivity, and in some cases epilepsy, we reasoned that MCPH proteins may have additional roles in postmitotic neurons, during synaptogenesis and synaptic transmission. Also, neurodevelopmental disorders associated with intellectual disability and neuropsychiatric conditions are often associated with defects in dendritic arborization and spine formation. We have therefore addressed whether loss of Cdk5rap2 as seen in MCPH3 affects the function of differentiated neurons in the neocortex by performing morphological and electrophysiological studies on the established MCPH3 mouse model, *Cdk5rap2* mutant or *Hertwig's anemia* mice (*an/an*). Our results demonstrate that Cdk5rap2 is essential for the maturation of the dendritic arbor and its synaptic connectivity and affects dendritic structure and synaptic connectivity in the mature brain.

2. Results

2.1. Preserved neocortical layer organization but thin upper layers

To address the role of Cdk5rap2 in mature neurons, we used the established *Cdk5rap2* mouse model (*Hertwig's anemia* mice (*an/an*)) (Lizarraga et al., 2010). *Cdk5rap2* mutant mice (*an/an*) display reduced overall brain size. Neocortical area was reduced to 46% and parietal cortical thickness to 67% (Fig. 1) at birth, in line with the findings reported by (Lizarraga et al., 2010). These structural changes persisted into adulthood (reduction in neocortical area to 50% and parietal cortical thickness to 68%; Fig. 1) and were associated with a strong reduction in the total number of cells in the neocortex of P0 and adult *an/an* mice (Fig. 2A and B).

Cortical layer organization was grossly undisturbed, as revealed by immunostaining with the layer 2–4 marker Cux1 and the layer 5–6 marker Ctip2 (Fig. 2A). While both $Cux1^+$ upper layers and $Ctip2^+$ deep layers were thinner (Fig. 2C), only the relative thickness of upper layers with respect to the total cortical thickness was reduced in P0 and adult *an/an* mice (Fig. 2C and Table S1). The relative thickness of deep layers with respect to total cortical thickness remained unchanged (Fig. 2C). Cell counts per view-field were reduced for $Cux1^+$ and $Ctip2^+$ neocortical neurons (Fig. 2D and Table S1). However, the relative number of both $Cux1^+$ and $Ctip2^+$ neocortical neurons (Fig. 2D) with respect to total $DAPI^+$ nuclei was not changed, suggesting that neuronal cell fate is unaltered. Together, these findings indicate that despite the large reduction in cell numbers and cortical area, cortical architecture remains relatively undisturbed.

2.2. Reduced dendritic complexity of layer 2/3 pyramidal neurons

We next analyzed the dendritic tree of layer 2/3 neocortical neurons of adult *an/an* and littermate +/+ mice in Golgi stained brain sections. We quantified the dendritic complexity of individual neurons using Sholl analysis (SHOLL, 1953). Mutant *Cdk5rap2* in *an/an* mice is associated with a downward shift of the Sholl curve for both apical and basal dendrites of layer 2/3 pyramidal neurons, indicating a marked reduction in the complexity of these dendrites (Fig. 3A, B and Fig. S2). In line, although the number of primary dendrites were similar (+/+ = 5.3 ± 0.2 *vs.* *an/an* = 4.9 ± 0.2 dendrites, $p = .2$, TT), numbers of secondary and tertiary dendrites were reduced in *an/an* (secondary: +/+ = 10.4 ± 0.3 *vs.* *an/an* = 8.8 ± 0.3 dendrites, $p < .002$, TT; tertiary: +/+ = 18.4 ± 1.3 *vs.* *an/an* = 10.5 ± 0.8 dendrites, $p < .0001$, TT; $n = 44$ +/+ and 39 *an/an* neurons from 6 +/+ and 4 *an/an* animals; Fig. 3B).

As neuronal surface area and input resistance are inversely proportional, the reduction in dendritic complexity could alter the intrinsic properties of *an/an* layer 2/3 neocortical neurons. We therefore performed whole cell patch clamp recordings on these neurons. Indeed, when compared to control neurons, *an/an* neurons showed an increased input resistance ($R_{in+/+}$ = 81.5 ± 8.6 MΩ, $n = 15$ *vs.* $R_{inan/an}$ = 153.5 ± 15.1 MΩ, $n = 17$, $p < .001$, MWU, Fig. 3C) while resting membrane potential remained similar ($V_{M+/+}$ = −79.1 ± 2.4 mV, $n = 14$ *vs.* $V_{Man/an}$ = −74.9 ± 2.5 mV, n = 10, $p = .1$, MWU). Accordingly, neuronal membrane capacitance was smaller in *an/an* ($C_{+/+}$ = 125.7 ± 11.3 pF *vs.* $C_{an/an}$ = 94.9 ± 6.8 pF, $p < .03$, MWU). As a consequence, the rheobase, *i.e.* the minimal current amplitude for action potential induction, decreased ($I_{rheo+/+}$ = 295.4 ± 23.6 pA, $n = 13$ *vs.* $I_{rheoan/an}$ 186.9 ± 44.3 pA, n = 13, $p = .04$, TT, Fig. 3E and F) and neuronal gain, given by the slope of the F/I relationship, increased ($F/I_{slope+/+}$ = 115.5 ± 14.9 AP/nA, $n = 14$ *vs.* $F/I_{slopean/an}$ = 159.6 ± 18.9 AP/nA, $n = 13$, $p = .08$, TT, Fig. 3E and G). Thus, our data imply that the reduced dendritic arborization of *an/an* neurons is associated with intrinsic pro-excitatory neuronal properties. While reduced dendritic arborization may impact on incoming dendritic signals by reducing the catchment area but increasing the electrotonic compactness (Spruston et al., 1993), the latter properties putatively privilege small and remote inputs.

2.3. Increased spine density, excitatory synapse number, and spontaneous glutamatergic transmission

Our morphological findings and the fact that MCPH patients can suffer from hyperactive behavior and seizures prompted us to study dendritic spine and synapse properties of layer 2/3 neurons in adult *an/an* mice. We first analyzed dendritic spines in Golgi-stained pyramidal neurons and found an increase in the density of spines along apical and basal dendrites (+/+ = 0.58 ± 0.04 μm^{-1} *vs.* *an/an* = 0.76 ± 0.03 μm^{-1}, $p = .0007$, TT, Fig. 3H and I). We next assessed whether spine morphology was altered in the mutants. We detected a significant increase in the number of thin-shaped "immature" spines in *an/an* mice compared to +/+ littermates (+/+ = 16.2 ± 2.5% *vs.* *an/an* = 28.5 ± 3.2%, $p < .005$, TT, Fig. 3H and I). Thin spines, containing long necks and small spine heads, are thought to represent immature spines (Dailey and Smith, 1996). To address whether the increase in spine density and altered spine morphology results in a change in excitatory transmission, we recorded spontaneous excitatory postsynaptic currents (sEPSCs) of layer 2/3 pyramidal neurons in *ex-vivo* adult brain slices (Fig. 3J). sEPSCs mainly correspond to spontaneous presynaptic glutamate vesicle release (Schuster et al., 2015), since spontaneous action potentials in layer 2/3 neurons in slices are unlikely events. In accordance with the elevated spine density we found an increase in the total excitatory charge transfer ($Q_{T+/+}$ = 1010.4 ± 135.3 fC, $n = 15$ *vs.* $Q_{Tan/an}$ = 1969.2 ± 460.2 fC, $n = 14$, $p < .05$, MWU, Fig. 3K) mainly due to an augmented sEPSCs frequency ($f_{+/+}$ = 18.1 ± 0.8 events/s, $n = 15$ *vs.* $f_{an/an}$ = 29.4 ± 1.6 events/s, $n = 14$, $p < .0001$, TT, Fig. 3L), since sEPSC kinetics were similar (decay: $\tau_{+/+}$ = 7.8 ± 0.6 ms, $n = 15$ *vs.* $\tau_{an/an}$ = 8.1 ± 0.8 ms, $n = 14$, $p = .6$, MWU). The increase in frequency might be in part due to the reduced neuronal size in *an/an* mice, making them electrically more compact and less leaky (Spruston et al., 1993).

Most of the additional spines in the mutant displayed "immature" thin spine morphology. Since spine head width has been correlated to the level of AMPA receptors, this could suggest a reduced number of AMPARs per spine (Matsuzaki et al., 2001). In our study mean EPSC amplitude and amplitude density, as indirect measures of AMPA receptor number in the postsynaptic density (Nair et al., 2013) did not differ between groups ($I_{+/+}$ = 10.5 ± 0.6 pA, $n = 15$ *vs.* $I_{an/an}$ = 8.8 ± 0.7 pA, $n = 14$, $p = .09$, TT, Fig. 3M, inset; $I/C_{+/}$

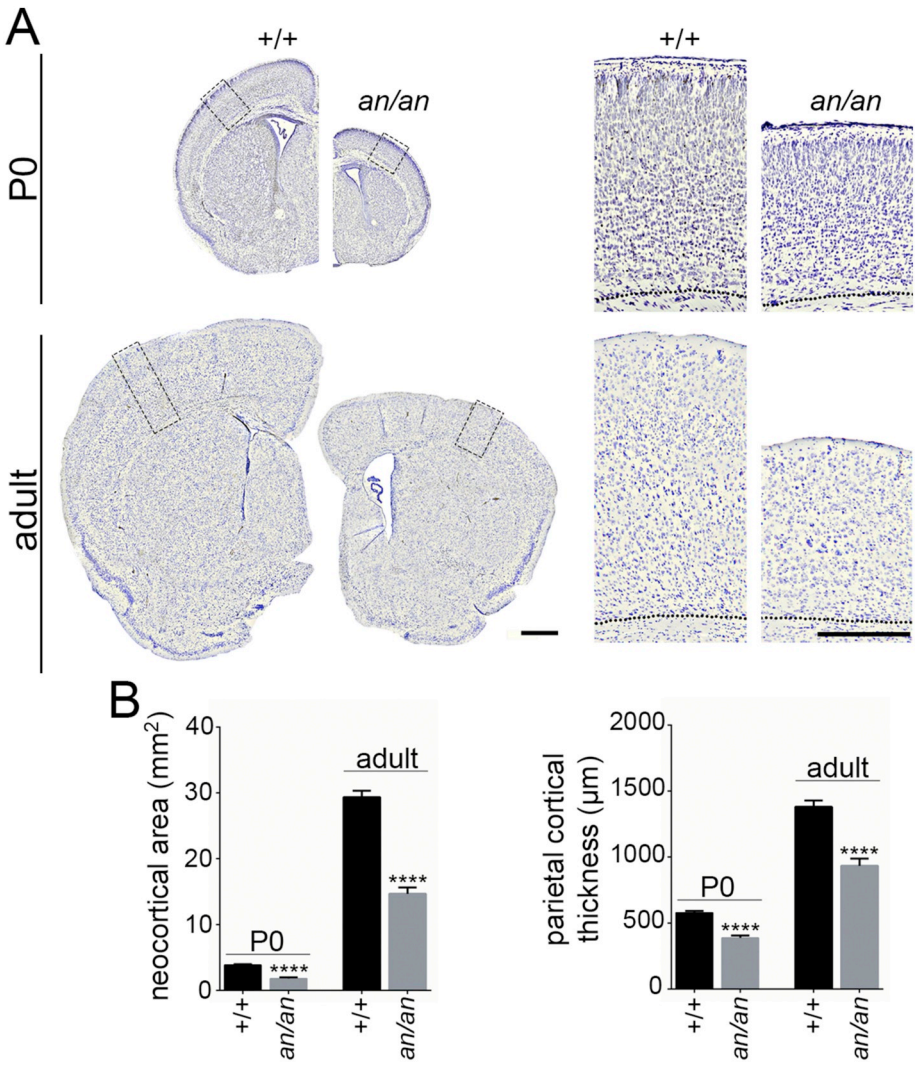

Fig. 1. Microcephaly with pronounced cortical thinning in *an/an* mice. (A) Coronal brain sections of P0 and adult littermate animals with parietal cortex sections magnified on the right side (Nissl staining, scale bars 500 µm). (B) Reduction of the neocortical area and parietal cortical thickness in *an/an* mice. Throughout these graphs $n = 8$ animals/group and error bars indicate S.E.M., TT, $^{**}p < .01$, $^{****}p < .0001$. For age as additional between subject factor see ANOVA at table S1.

$_{+} = 0.092 \pm 0.009$ pA/pF, $n = 15$ *vs.* $I/C_{an/an} = 0.097 \pm 0.008$ pA, $n = 14$, $p = .65$, MWU), excluding an overall postsynaptic phenotype in *an/an* neurons.

Survival to adulthood is a very rare event for *an/an* mice. To test whether the changes in cell morphology was directly caused by the loss of gene function or rather the result of secondary compensatory effects, we investigated layer 2/3 neuronal activity in *an/an* mice at an early stage of synaptogenesis using *ex-vivo* P6/7 brain slices. At this stage of development, we did not observe significant changes in membrane resistance, neuronal excitability ($R_{in+/+} = 598.6 \pm 50.7$ MΩ, $n = 29$ *vs.* $R_{inan/an} = 657.9 \pm 53.6$ MΩ, $n = 35$, $p = .45$; $I_{rheo+/+} = 29.2 \pm 3.7$ pA *vs.* $I_{rheoan/an} = 35.8 \pm 5.6$ pA, $p = 1$, MWU; $FI_{slope+/+} = 334.5 \pm 21.5$ AP/nA, n = 29 *vs.* $FI_{slopean/an} = 421.1 \pm 44.8$ AP/nA, n = 35, $p = .2$, MWU; $V_{M+/+} = -72.6 \pm 1.1$ mV, $n = 22$ *vs.* $V_{Man/an} = -68.9 \pm 1.7$ mV, $n = 27$, p = .2 Fig. 4A – D) or neuronal membrane capacitance ($C_{+/+} = 75.1 \pm 5.4$ pF *vs.* $C_{an/an} = 74.5 \pm 4.1$ pF, $p = .99$, MWU). This indicates comparable electrotonic compactness at this stage, enabling us to investigate electrophysiological differences independent of gross morphological changes. Excitatory synaptic drive was already elevated in the mutant as evident by the 48% increase in total excitatory charge transfer ($Q_{T+/+} = 93.3 \pm 16.6$ fC, $n = 23$ *vs.* $Q_{Tan/an} = 138.6 \pm 18.3$ fC, $n = 28$, $p < .08$, MWU; Fig. 4F) and 53% increase in sEPSC frequency ($f_{+/+} = 2.18 \pm 0.22$ events/s, $n = 29$ *vs.* $f_{an/an} = 3.33 \pm 0.27$ events/s, $n = 38$, $p = .008$, MWU; Fig. 4E and G). This increase in frequency was not accompanied by a change in amplitude ($I_{+/+} = 6.24 \pm 0.39$ pA, $n = 29$ *vs.* $I_{an/an} = 5.84 \pm 0.31$ pA, $n = 38$, $p = .3$, MWU; Fig. 4H), amplitude density ($I/C_{+/+} = 0.087 \pm 0.005$ pA/pF, $n = 29$ *vs.* $I/C_{an/an} = 0.084 \pm 0.005$ pA, $n = 38$, $p = .89$, MWU) or kinetics (decay: $\tau_{+/+} = 7.8 \pm 0.5$ ms, $n = 29$ *vs.* $\tau_{an/an} = 8.1 \pm 0.6$ ms, $n = 38$, $p = .7$, TT).

Changes in sEPSC frequency in P6-7 *an/an* mice are unlikely due to the detection of more events from distal dendrites because electrical compactness was similar in both genotypes. The increase could be mediated by changes in spontaneous presynaptic firing (but see TTX-experiments under 2.5) or may be linked to presynaptic vesicle release probability (del Castillo and Katz, 1954). We therefore evoked paired pulse responses in layer 2/3 neocortical neurons but found no alteration in the paired pulse ratio of *an/an* cells (Fig. 4I and J), suggesting that presynaptic release probability is unaffected. Finally, immunohistochemical staining for pre- (VGlut1) and postsynaptic (PSD95) markers revealed a 66% increase in VGlut1/PSD95-positive synapses already at P6/7 in *an/an* layer 2/3 neurons (Fig. 4K and L). Taken together, these results point towards an increase in excitatory drive of layer 2/3 pyramidal neurons in *an/an* mice regardless of their age or severity of alteration (as indicated by early death *vs.* survival).

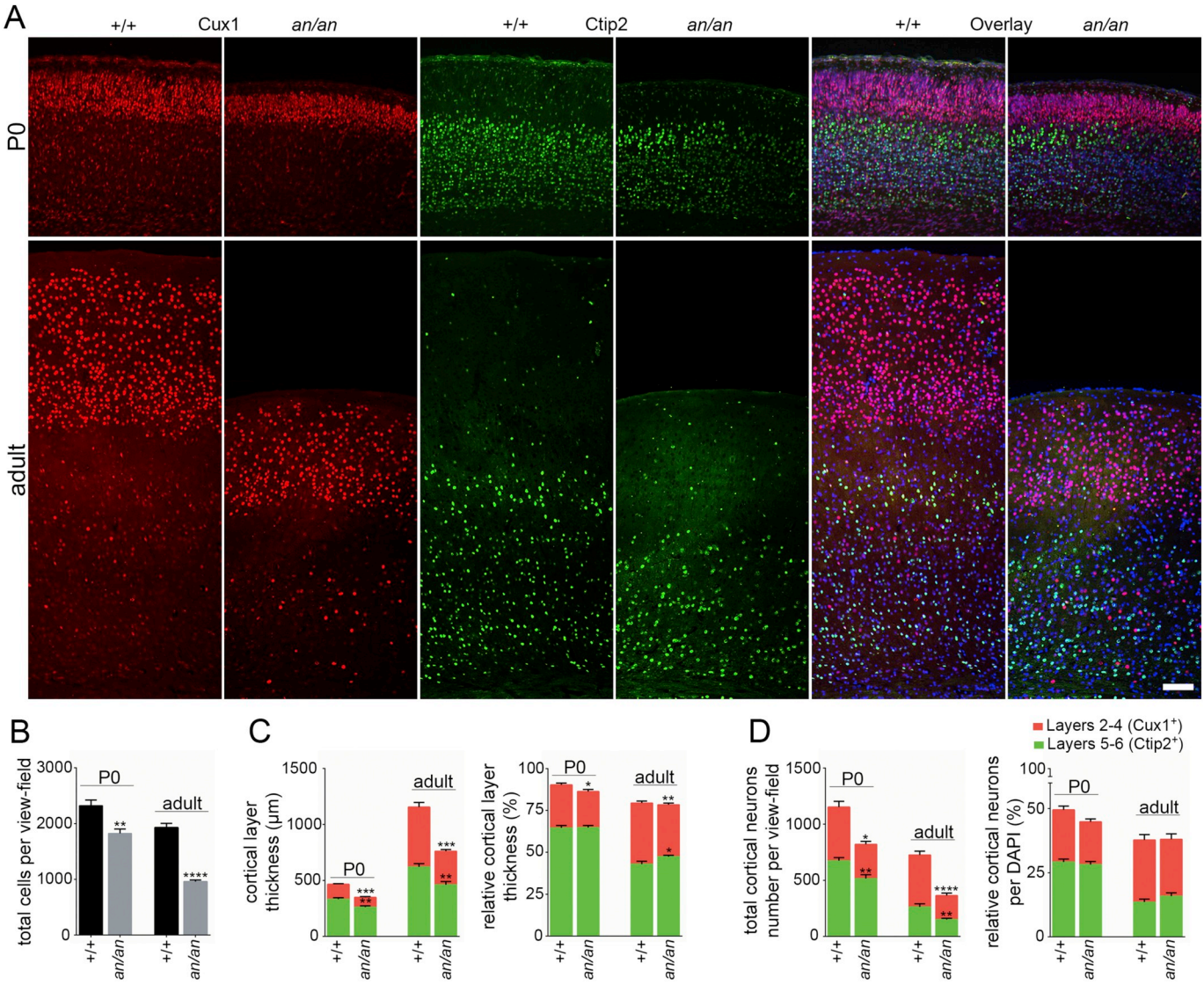

Fig. 2. Preserved neocortical layer organization despite reduced thickness of upper cortical layers in *an/an* mice. (A) Coronal brain sections of P0 and adult littermate animals stained for upper layer marker Cux1 (layers 2–4) and deeper layer marker Ctip2 (layers 5–6) (immunofluorescence images, scale bar 100 µm). (B) Reduction of total DAPI$^+$ nuclei per view-field in *an/an* mice. (C) While the Cux1$^+$ upper layers and Ctip2$^+$ deep layers are thinner, only the relative thickness of upper layers with respect to the total cortical thickness mice was reduced in *an/an* mice. The relative thickness of the deep layers with respect to the total cortical thickness was similar. (D) Reduction of the Cux1$^+$ and Ctip2$^+$ cortical layer neurons per view-field in *an/an* mice *versus* +/+ littermates without reduction in the relative number of both layers. Throughout these graphs $n = 7$ animals/group and error bars indicate S.E.M., TT, $p < .05$, $^{**}p < .01$, $^{***}p < .001$, $^{****}p < .0001$. For age as additional between subject factor see ANOVA at table S1.

2.4. Minor influence of Cdk5rap2 on dendritic complexity or excitatory transmission in cultured neocortical pyramidal neurons

Altered Cdk5rap2 function may contribute, in a cell intrinsic fashion, to reduced dendritic complexity and elevated excitatory drive of *an/an* mice layer 2/3 neurons. Cdk5rap2 has been shown to interact with chromatin associated Cdc20-anaphase promoting complex (Cdc20-APC) protein (Kraemer et al., 2011; Zhang et al., 2009) that can influence dendritic development (Kim et al., 2009). Therefore, we investigated the effect of Cdk5rap2 loss of function *in vitro*. We first used autaptic (*i.e.* singly cultured neurons) primary neuronal cultures from newborn +/+ and *an/an* cortices that allow for detailed quantification of synaptic properties. Neurons derived from *an/an* cultures had a reduced soma size ($A_{+/+} = 148.6 \pm 7.7\,\mu m^2$, $n = 28$ *vs.* $A_{an/an} = 126.3 \pm 5.6\,\mu m^2$, $n = 38$, $p = .02$, TT). We found no significant change in the total length of dendrites ($L_{d+/+} = 962.9 \pm 92.8\,\mu m$, $n = 28$ *vs.* $Ld_{an/an} = 878.8 \pm 74.9\,\mu m$, $n = 36$, $p = .7$, MWU). The axonal length was reduced by nearly 30% when compared to those from +/+ cultures ($L_{aan/an} = 986.9 \pm 159.8\,\mu m$, $n = 23$ *vs.* $L_{a+/+} = 1314.1 \pm 172.1\,\mu m$, $n = 17$, $p = .07$, MWU, Fig. 5A and C). However, numbers of primary dendrites (+/+: 5.4 ± 0.6, $n = 20$; *an/an*: 5.7 ± 0.4, $n = 31$, $p = .46$, MWU) and dendritic tips (+/+: 20.9 ± 2.1, n = 20 *an/an*: 22.0 ± 1.6, $n = 31$, $p = .7$, TT) did not differ between the groups, resulting in a comparable branching index (+/+: 4.2 ± 0.4, n = 20, *an/an*: 5.7 ± 0.25, $n = 31$, $p = .57$, TT, Fig. 5A and B).

We next analyzed the synaptic transmission of glutamatergic autaptic neurons but found no significant difference in evoked responses (EPSCs; $I_{+/+} = 5.54 \pm 0.67$ nA, $n = 65$ *vs.* $I_{an/an} = 5.15 \pm 0.67$ nA, $n = 54$, $p = .64$, MWU, Fig. 5D) nor in mEPSC rates or amplitudes between +/+ and *an/an* mouse neurons ($f_{+/+} = 2.3 \pm 0.4$ events/s, $n = 52$ *vs.* $f_{an/an} = 2.7 \pm 0.4$ events/s, $n = 45$, $p = .3$, MWU; $I_{+/+} = 24.5 \pm 1.7$ pA, $n = 52$ *vs.* $I_{an/an} = 23.6 \pm 1.3$ pA, $n = 45$, $p = .9$, MWU; Fig. 5H to J). Utilizing responses induced by hypertonic solution,

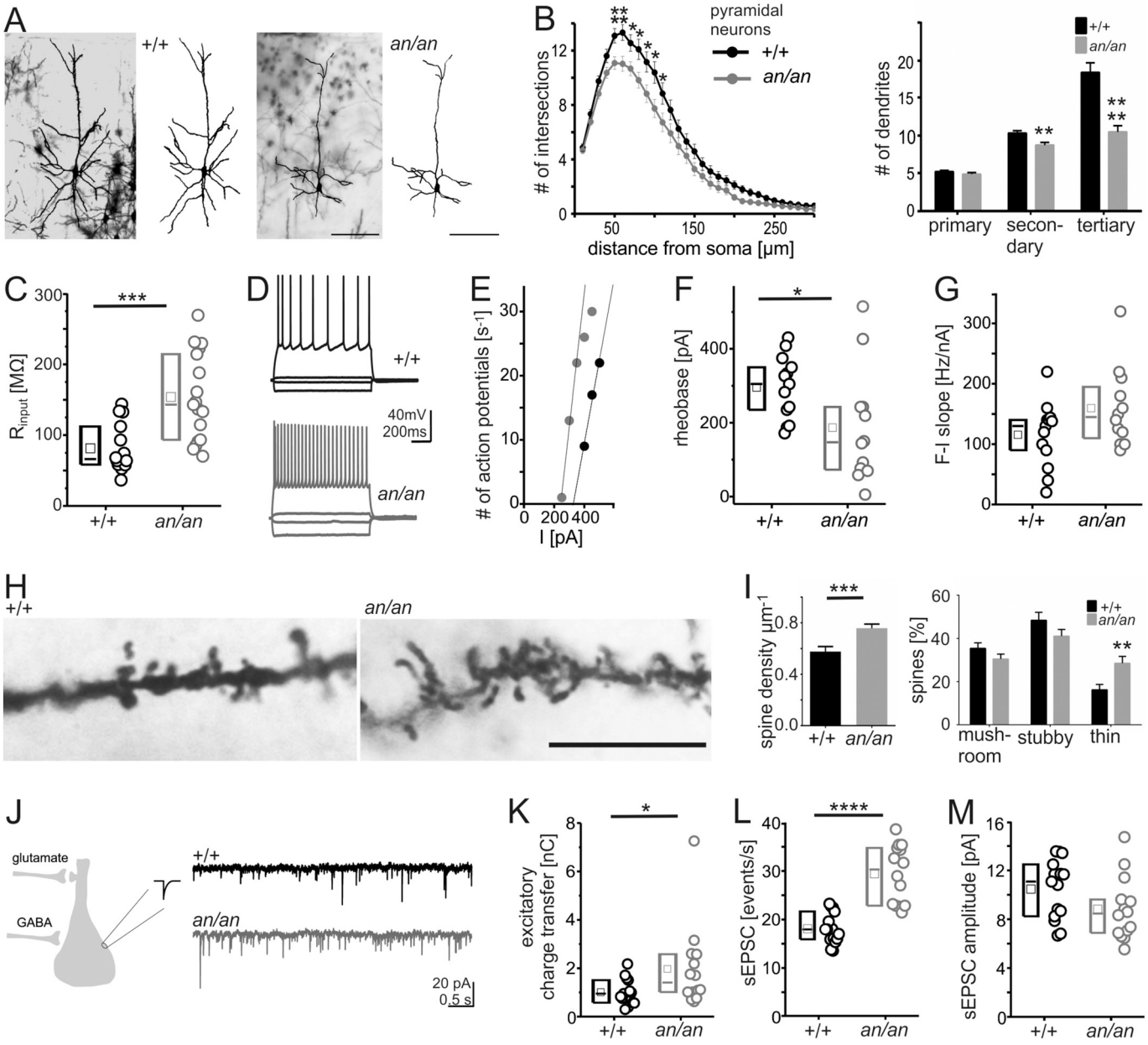

Fig. 3. Distinctive morphological and physiological characteristics of layer 2/3 pyramidal neurons from *an/an* mature neocortex. (A and B) Reduced dendritic complexity in photomicrographs / reconstructed neurons (A, Golgi staining, scale bar 100 µm) as shown by less dendritic intersections 50–110 µm from the soma and a reduction of the numbers of secondary and tertiary dendrites in *an/an* mice (B, Sholl analysis, $n = 44$ +/+ and 39 *an/an* neurons from 6 +/+ and 4 *an/an* animals). (C) Input resistance of an/an neurons was increased. (D) Exemplary voltage responses to rectangular current injections (−200, ± 50 and 400 pA) depicting firing behavior (D) and the relation of elicited action potentials and the current injected (E). (F and G) Population data showing shifted neuronal offset (F) and a trend towards an increased gain in *an/an* neurons (G). (H) Magnified image of secondary basal dendrites (Golgi staining, scale bar 10 µm). (I) Average spine density was increased (left) with a larger proportion of thin-shaped immature spines in *an/an* mice (right, $n = 410$ +/+ and 373 *an/an* spines counted in 34 (+/+) and 30 (*an/an*) 20 µm long dendritic segments from 5 animals/group). (J) Scheme and example traces of sEPSCs recordings in neurons voltage clamped at -60 mV. (K) Box plots showing an increased total excitatory charge transfer in *an/an* mice due to increased sEPSCs frequency (L). (M) Average amplitudes were not altered. Serial resistance ($R_{s+/+} = 9.8 \pm 0.7$ MΩ *vs.* $R_{san/an} = 11.0 \pm 0.6$ MΩ, $p = .1$; not shown) was comparable. Population data for *E*-G and K-M are from 15 +/+ and 14 *an/an* neurons from 4 animals / group; age: P30 – P80). Boxes in this and the following figures represent 25–75% plots, means and medians are depicted by an open square and a horizontal line, respectively.

we next determined the size of the readily releasable pool (RRP = the amount of primed synaptic vesicles; (Rosenmund and Stevens, 1996)) in *an/an* compared to +/+ neurons and found, consistent with the unchanged evoked response, no alteration between wildtype and mutant neurons ($RRP_{+/+} = 307.2 \pm 51.4$ pC, $n = 51$ *vs.* $RRP_{an/an} = 416.5 \pm 71.5$ pC, $n = 44$, p = .3, MWU; Fig. 5E and F). The vesicular release probability (Pvr), as calculated by comparing evoked response and RRP size, was also comparable between +/+ and *an/an* neurons ($Pvr_{+/+} = 11.7 \pm 0.9\%$, n = 51 *vs.* $Pvr_{an/an} = 10.6 \pm 0.9\%$, n = 44, p = .9, TT, Fig. 5G).

We further examined synapse formation on cortical neurons in dissociated cultures and found no differences. In detail, the density of glutamatergic presynaptic punctae was comparable (Fig. 5K; VGlut1; +/+ = 3140 ± 249 puncta/0.15 mm^2, $n = 38$ *vs.* *an/an* = 3487 ± 300 puncta/0.15mm^2, $n = 37$, $p = .4$, MWU; from 3 independent cultures). Taken together, our results from the cultured neurons imply that

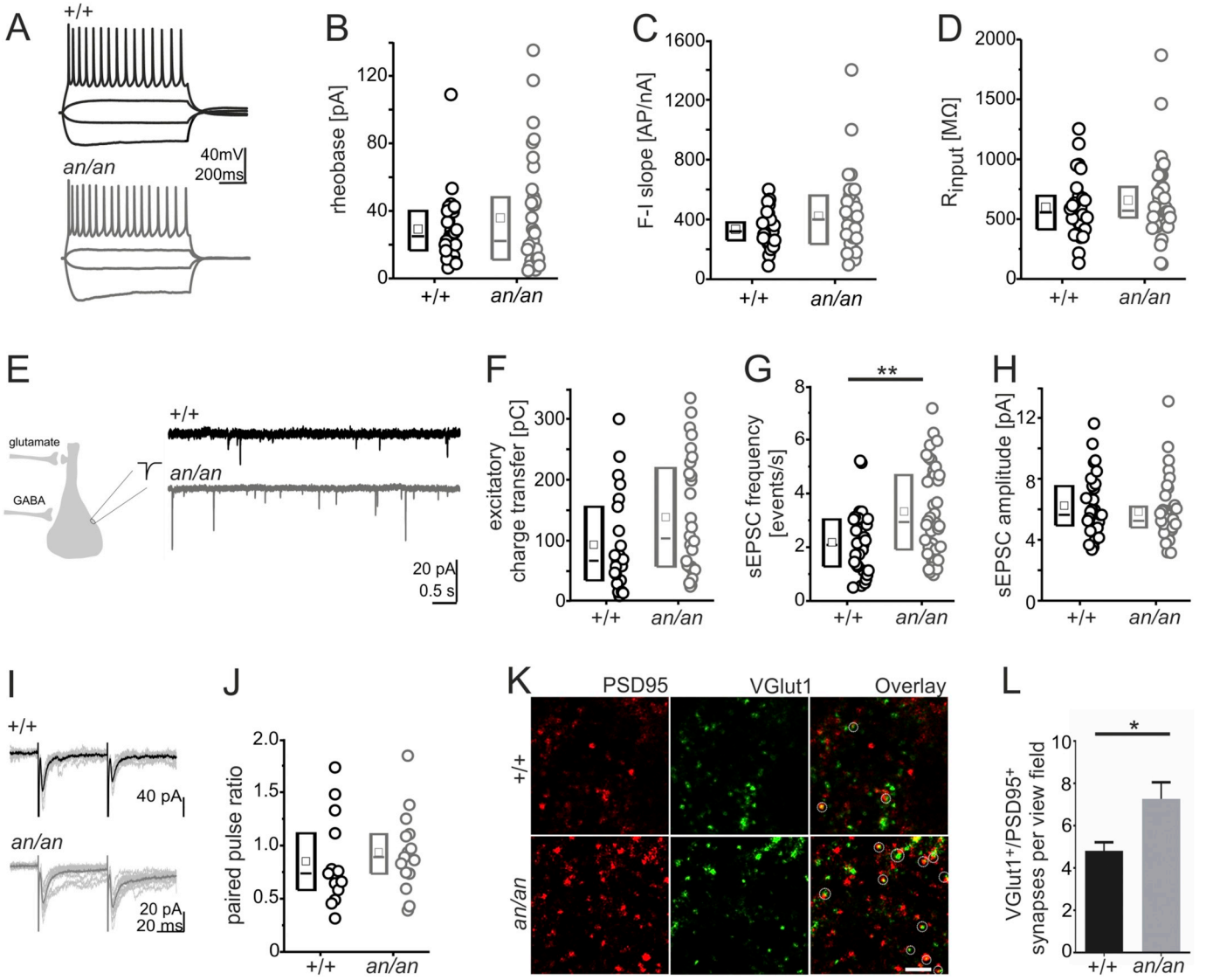

Fig. 4. Increased excitatory synapse number and frequency of sEPSCs of layer 2/3 neocortical pyramidal neurons at onset of synaptogenesis (P6/7). (A) Voltage changes of exemplary +/+ (top) and *an/an* (bottom) neurons to rectangular current injections of −100, ± 25 and 100 pA. (B and C) Population data on neuronal offset (B) and gain (C) revealed no differences. (D) Input resistance did not vary between +/+ and *an/an* neurons. (E) Scheme and example traces for sEPSC recordings in neurons voltage clamped at -60 mV. (F and G) Box plot graphs displaying values from 29 +/+ and 38 *an/an* neurons from 4 animals/group, showing a trend towards increased total excitatory charge transfer in *an/an* mice (F) and an increase in sEPSC frequency in neurons from *an/an* mice (G). (H) Average amplitudes remained unchanged. Serial resistance ($Rs_{+/+}$ = 9.1 ± 0.5 MΩ *vs.* $Rs_{an/an}$ = 8.8 ± 0.4 MΩ, p = .57; not shown) was similar. (I) Synaptic responses evoked by electrical stimulation overlay of 10 individual traces recorded with 20 s intervals and a highlighted average trace. (J) population data of paired pulse ratio ($PPR_{+/+}$ = 0.85 ± 0.11 *vs.* $PPR_{an/an}$ = 0.93 ± 0.09, p = .6). (K) 100 μm^2 images of the upper layer of the parietal cortex at upper layer areas from littermate animals stained for VGlut1 (excitatory-presynaptic) and PSD95 (postsynaptic) markers. Overlay depicts VGlut1/PSD95 positive synapses (dotted circles) (confocal images, scale bar 2 μm). (L) The number of VGlut1/PSD95 positive synapses at layer 2/3 areas is increased in *an/an* mice (+/+ = 4.8 ± 0.4 *vs. an/an* = 7.3 ± 0.8; n = 18 images from 4 +/+ animals and 28 images from 5 *an/an* animals).

changes induced by *Cdk5rap2* mutation are not entirely cell intrinsic and require *in-vivo* like neuron-neuron interactions. Note that these results do not exclude an astrocytic malfunction in *an/an*, because both, autaptic and continental neuronal cultures were grown on non-mutated feeder astrocytes.

2.5. Decreased inhibitory tone in ex-vivo slices of Cdk5rap2 mutants

Given the observed increased excitatory drive at the soma of pyramidal *Cdk5rap2* mutant neurons *ex-vivo* but not in singly cultured neurons and the known control of pyramidal neurons by inhibitory neurons, we again drew upon brain slice experiments to analyze the importance of neuronal interaction for the Cdk5rap2 phenotype. We first examined the inhibitory tone in *ex-vivo* brain slices by quantifying miniature inhibitory postsynaptic currents (mIPSC) (Fig. 6A). At P6-7, we found that the *Cdk5rap2* mutation is associated with decreased inhibitory charge transfer ($Q_{T+/+}$ = 126.3 ± 13.5 fC, n = 30 *vs.* $Q_{Tan/an}$ = 102.4 ± 12.9 fC, n = 32, p < .03, MWU, Fig. 6B). A comparison of frequency and amplitude of mIPSC events showed that the decreased tone was most likely due to the decreased frequency of events ($f_{+/+}$ = 1.40 ± 0.05 events/s *vs.* $f_{an/an}$ = 1.04 ± 0.05 events/s, p < .0001, MWU) because mIPSC amplitude ($I_{+/+}$ = 11.36 ± 0.95 pA, n = 30 *vs.* $I_{an/an}$ = 12.28 ± 0.94 pA, n = 32, p = .2, MWU, Fig. 6C and D), amplitude density ($I/C_{+/+}$ = 0.129 ± 0.009 pA/pF *vs.* $I/C_{an/an}$ = 0.131 ± 0.009 pA/pF, p = .86, TT), mIPSC kinetics (decay: $\tau_{+/+}$ = 8.34 ± 0.21 ms, n = 30 *vs.* $\tau_{an/an}$ = 8.62 ± 0.46 ms, n = 32, p = .8, MWU) and neuronal membrane capacitance ($C_{+/+}$ = 90.2 ± 13.1 pF *vs.* $C_{an/an}$ = 89.0 ± 8.3 pF, p = .7, MWU) were

similar in both genotypes. This indicates that less inhibitory synapses are formed on pyramidal neurons already in emerging neural networks, which suggests that the density and/or axonal tree formation of inhibitory neurons is impaired.

The ability of synapse formation itself was not disturbed in cultured GABAergic autaptic neurons (Fig. 6E) of *an/an* mice as synaptic transmission was comparable in the two groups. In particular, evoked responses were similar in both genotypes (IPSCs; $I_{+/+}$ = 4.81 ± 1.41 nA, n = 8 *vs.* $I_{an/an}$ = 4.13 ± 2.57 nA, *n* = 15, *p* = .62, TT, Fig. 6F and G). Consistent with the unchanged evoked response, RRP size ($RRP_{+/+}$ = 2592.8 ± 650.3 pC, *n* = 8 *vs.* $RRP_{an/an}$ = 2179.7 ± 274.1 pC, *n* = 14, *p* = .6, 77; Fig. 6H and I) and Pvr ($Pvr_{+/+}$ = 12.1 ± 3.0%, *n* = 8 *vs.* $Pvr_{an/an}$ = 16.5 ± 2.6%, *n* = 44, *p* = .9, TT, Fig. 6J) were also comparable between +/+ and *an/an* mice. Finally, mIPSC rates or amplitudes of +/+ and *an/an* mouse neurons ($f_{+/+}$ = 0.7 ± 0.2 events/s, *n* = 4 *vs.* $f_{an/an}$ = 0.9 ± 0.4 events/s, *n* = 9, *p* = .5, MWU; $I_{+/+}$ = 32.7 ± 9.2 pA, *n* = 4 *vs.* $I_{an/an}$ = 27.9 ± 4.5 pA, *n* = 9, *p* = .8, MWU; Fig. 6K – M) and the number of inhibitory synapses (VGat; +/+ = 2513.1 ± 197.2 puncta/0.15 mm^2, *n* = 38 *vs. an/an* = 3007.5 ± 257.9 puncta/0.15 mm^2, *n* = 37, *p* = .2, MWU, Fig. 5J) were similar.

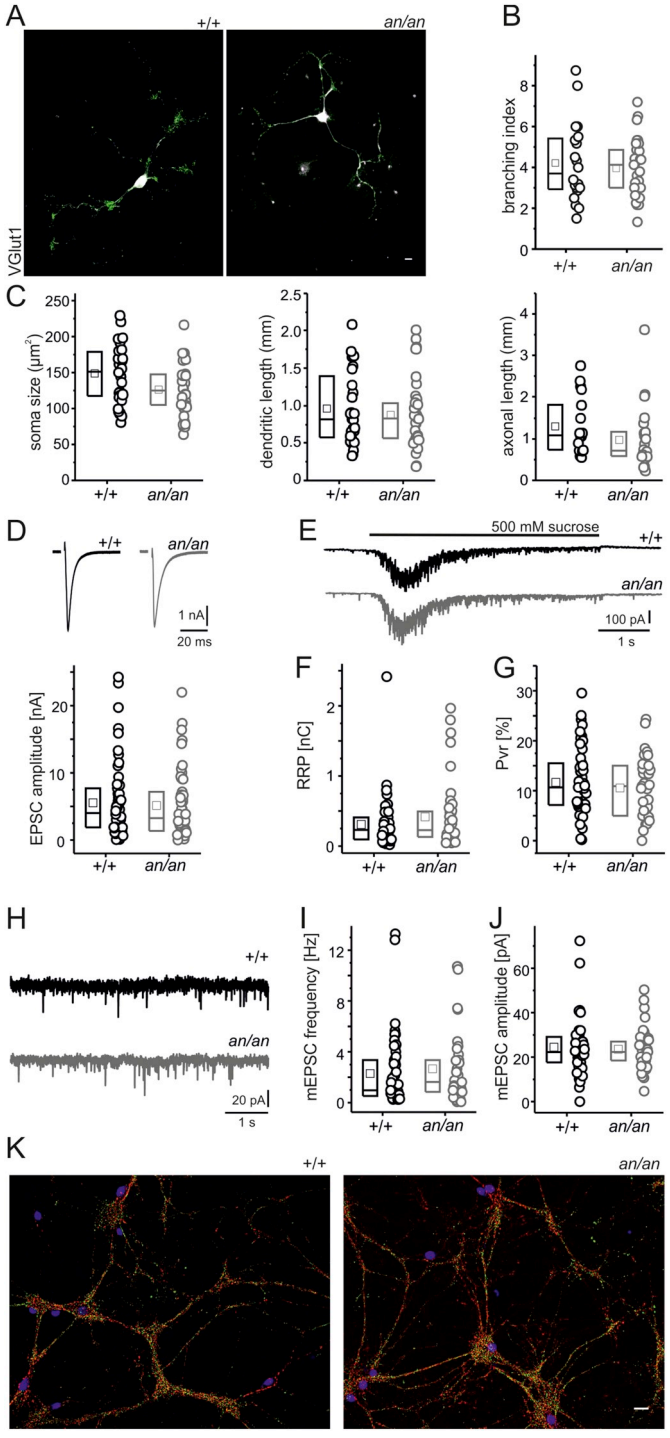

Fig. 5. Neocortical pyramidal neurons derived from *an/an* and +/+ mice display a comparable phenotype *in vitro*. (A) Photomicrographs of cultured neurons stained for neuronal cytoskeleton by microtubule associated protein (Map2 – white, all panels) and VGlut1 (green), scale bar: 10 µm. (B) Box plots of branching index estimated by the ratio of counts of dendritic tips / primary dendrites confirm a lack of alteration in branching patterns. (C) Box plots illustrating soma size, dendritic length and axonal length of autaptic cortical excitatory neurons. (D) Traces of excitatory postsynaptic currents (top) after a 2 ms depolarization (EPSC) and population data of EPSC amplitudes from 65 +/+ (black) and 54 *an/an* (grey) autaptic cortical neurons. (E) Responses from +/+ (black) and *an/an* (grey) cortical neurons during 500 mM sucrose application for 5 s. (F) Box plot of readily releasable pool (RRP) and (G) average vesicular release probability (P_{vr} = EPSC charge / RRP charge) in autaptic +/+ (51) and *an/an* (44) cortical excitatory neurons. (H) Traces of mEPSC from +/+ (black) and *an/an* (grey) neurons. (I and J) Box plots of mEPSC frequencies (I) and mEPSC amplitudes (J, +/+: 47 neurons; *an/an*: 43 neurons). Data was collected from 2 independent cultures. (K) Examples of continental (high density) cultures stained for presynaptic markers VGlut (green), VGat (red) and the nuclear marker DAPI (blue), scale bar: 25 µm. (For interpretation of the references to colour in this figure legend, the reader is referred to the web version of this article.)

In search for a morphological correlate of decreased inhibition in *Cdk5rap2* mutant mice, we stained the cortex for GABA, a marker for interneurons (Uematsu et al., 2008) that is also expressed in astrocytes (Yoon and Lee, 2014). However, astrocytes do not substantially contribute to the $GABA^+$ cells at P6–7 (Fig. S4). The total number of $GABA^+$ cells in P6–7 *an/an* mice was smaller ($GABA^+_{+/+}$ = 71.0 ± 5.2 neurons per view-field, *n* = 6 animals *vs.* $GABA^+_{an/an}$ = 50.5 ± 7.1 neurons per view-field, n = 3 animals, *p* = .048, MWU; Fig. 7A and B). This reduction matches the general diminution of the neocortex since the relative proportion of these neurons (compared to total $NeuN^+$ cells) was similar ($GABA^+/NeuN^+_{+/+}$ = 4.9 ± 0.5% n = 6 animals *vs.* $GABA^+/NeuN^+_{an/an}$ = 6.2 ± 0.6% n = 3 animals, *p* = .1, MWU; Fig. 7A and B). In contrast, we found a decrease in both the total number of $GABA^+$ interneurons in adult *an/an* mice ($GABA^+_{+/+}$ = 37.3 ± 5.2 neurons per view-field, *n* = 6 animals *vs.* $GABA^+_{an/an}$ = 7.8 ± 1.5 neurons per view-field, *n* = 4 animals, *p* = .0095, MWU; Fig. S3A and B) and in the relative proportion of these neurons ($GABA^+/NeuN^+_{+/+}$ = 2.7 ± 0.4%, *n* = 6 animals *vs.* $GABA^+/NeuN^+_{an/an}$ = 1.2 ± 0.2%, *n* = 4 animals, *p* = .0095, MWU; Fig. S3A and B). In line with the reduced mIPSC frequencies, layer 2/3 from P6–7 *an/an* mice showed a trend towards decreased numbers of $VGat^+$ presynaptic inhibitory terminals in comparison to +/+ littermates (+/+ = 110.3 ± 18.0 *vs. an/an* = 73.1 ± 8.2, *p* = .09, TT; Fig. 7C and D). By co-staining the same slices with VGlut1 and calculating the ratio of VGlut1 and VGat positive punctae we found a markedly increased morphological excitation to inhibition (E/I) ratio of layer 2/3 neurons in *an/an* mice (+/+ = 1.3 ± 0.2 *vs. an/an* = 2.4 ± 0.2, *p* = .003, TT; Fig. 7D) as a result of a decrease in inhibitory relative to excitatory (see also Fig. 4K and L) synapses. This is roughly in line with the functional E/I ratios calculated by dividing excitatory and inhibitory charge transfers (+/+ = 1.14 ± 0.3 *vs. an/an* = 1.6 ± 0.2, *p* = .056, MWU). The reduced inhibition (less mIPSCs and VGat positive terminals) is likely due to the decreased number of GABAergic synapses in the cortex, since neither inhibitory quantal amplitude nor IPSC decay kinetic was altered.

We reasoned that the reduced inhibitory influence observed in *an/an* neurons *ex-vivo* contributes to an elevated frequency of glutamatergic signals at the soma. If our hypothesis holds true, blocking

GABAergic transmission should level out the differences in the number of excitatory events between the groups (*i.e.* particularly increase the frequency of glutamatergic signals in wild-types, similar to finding in *Cdk5rap2* mutants). We therefore applied the $GABA_A$ receptor blocker bicuculline (20 μM) to block inhibition and the sodium channel blocker tetrodotoxin (1 μM) preventing increased pyramidal action potential firing induced by bicuculline (Turrigiano et al., 1998) and putative spontaneous interneuronal action potentials. Indeed, this treatment increased the frequency of excitatory events in +/+ (3.9 ± 0.4 to 5.5 ± 0.4 events/s, $n = 24$, $p = .02$, ANOVA-RM-B in +/+) but not in *an/an* littermates at P6/7 (5.4 ± 0.4 to 5.8 ± 0.4 events/s, $n = 22$, $p = 1$, ANOVA-RM-B in *an/an* neurons) (Fig. 7E–G). Note that in a subset of experiments TTX alone did not change PSC frequencies in general (2.6 ± 0.3 *vs.* 2.8 ± 0.3 events/s, $n = 17$, $p = 1$, ANOVA-RM-B) or in one of the genotypes (1.8 ± 0.2 *vs.* 1.9 ± 0.3 events/s, $n = 9$ in +/+, and 3.6 ± 0.4 *vs.* 3.8 ± 0.4 events/s, $n = 8$ in *an/an*, $p = 1$, ANOVA-RM-B, respectively). This also renders a contribution of increased presynaptic firing to the elevated sEPSC frequencies in *an/an* mice (see 2.3) unlikely. We cannot, however, rule out that even in the electrotonic compact neurons at P6-7 the increase in sEPSC frequency is caused by a redistribution of the same number of excitatory inputs causing more EPSCs to be detected somatically. Initial frequencies of sEPSC before blocking of $GABA_A$ receptors were again increased in *an/an* compared to wild-type neurons (Fig. 7F; $p = .04$, ANOVA-RM-B). Notably, the excitatory charge transfers ($Q_{T+/+} = 151.0 \pm 27.6$ fC, n = 24 *vs.* $Q_{Tan/an} = 115.2 \pm 16.3$ fC, $n = 22$, $p = .3$, ANOVA-RM-B) including mEPSC frequencies ($p = .6$), quantal mEPSC amplitudes ($I_{+/+} = 6.7 \pm 0.9$ pA, $n = 24$ *vs.* $I_{an/an} = 5.4 \pm 0.8$ pA, $n = 22$, $p = .5$) and mEPSC kinetics (decay: $\tau_{+/+} = 4.8 \pm 0.3$ ms, $n = 24$ *vs.* $\tau_{an/an} = 4.2 \pm 0.2$ ms, $n = 22$, $p = .2$, all ANOVA-RM-B) did not differ between neurons from +/+ and *an/an* animals after blocking inhibition. Neuronal membrane capacitance ($C_{+/+} = 70.8 \pm 4.0$ pF *vs.* $C_{an/an} = 84.8 \pm 9.8$ pF, $p < .09$, MWU) and amplitude density ($I/C_{+/+} = 0.088 \pm 0.010$ pA/pF, $n = 24$ *vs.* $I/C_{an/an} = 0.065 \pm 0.010$ pA, $n = 22$, $p = .51$, ANOVA-RM-B) were comparable in +/+ and *an/an* neurons. Together these results suggest that the elevated excitatory drive at the soma detected in *an/an* mice is related to reduced inhibitory $GABA_A$ mediated transmission.

3. Discussion

Reduced brain size in patients with MCPH has been attributed to an abnormal proliferation of neural progenitors. Here we show that Cdk5rap2 also regulates the differentiation of neocortical neurons and the establishment of the neocortical circuit.

We demonstrate that the profound developmental reduction in brain size, cortical thickness and neuron numbers in the *an/an* mouse model of MCPH3 (Lizarraga et al., 2010) persists into adulthood (Fig. 1). Brain size in itself does not necessarily imply dysfunctionality. Therefore, we investigated whether the malfunction of microcephaly-associated protein Cdk5rap2 results in additional cellular and functional defects that contribute to the neurologic phenotype. Perhaps our most striking finding is that the *Cdk5rap2* mutation impacts the establishment and function of neocortical circuits, whilst pyramidal cell fate specification and cortical layering remain grossly unaltered (Fig. 2). In particular, *an/an* mice are distinguished by an enhanced excitatory drive of neocortical pyramidal neurons during synaptogenesis and in adulthood. We performed multiple experiments to further dissect the underlying mechanism: (**1**) On the *in vitro* level of individual isolated neurons neither morphological nor physiological differences between neocortical neurons of *an/an* mice and their wild-type litters were present (Figs. 5 and 6). This finding suggests a dysfunction developing network (including astrocytes) rather than mere cell autonomous mechanisms. (**2**) In *ex-vivo* slices from adult *an/an* mice we found simplified dendritic arbors with increased thin “immature” spines to be accompanied by an increase in both intrinsic excitability and (extrinsic) excitatory drive on single layer 2/3 pyramidal neurons. (**3**) To address the question whether the increase in excitatory drive is a secondary effect, *i.e.*, results from increased intrinsic excitability, we investigated layer 2/3 neurons at an early stage of synaptogenesis. The overall increased excitatory drive in the mutants seems of primary synaptic origin, since the increased excitatory drive was not accompanied by a change in intrinsic excitability (Fig. 4). The increased excitatory drive was accompanied by reduced inhibition (Fig. 6). (**4**) In line with the electrophysiological data, we detected an increase overall number of excitatory synapses and a reduced number of inhibitory synapses in the cortex (Figs. 4 and 6). This imbalance in the number of excitatory to inhibitory synapses on a morphologic level in the cortex, however, does not specifically pinpoint the finding to pyramidal neurons. (**5**) Addressing the role of inhibition in the pathomechanism of MCPH, we found that blocking of GABAergic inhibition levels the excitatory drive of pyramidal neurons of *an/an* and wild-type littermates (Fig. 7), arguing that the increased excitatory drive is related to a primary lack of inhibition. We cannot exclude a contribution of astrocytic malfunction, although at P6-7 no obvious morphological differences were detected (Fig. S4). Altogether, we conclude that the increase in excitability is due to a shift in the balance of excitation and inhibition and that the predominant effect of Cdk5Rap2 mutation on the network level is loss of GABAergic tone onto pyramidal neurons.

Reduced inhibition might result either from a decrease in interneuron number or from a failure of interneurons to integrate into functional networks for instances by an impaired ability to form functional inhibitory synapses or both. We favor decreased inhibitory synapse formation as primary cause at early stages (Fig. 6) putatively resulting in reduced interneuron density at later stages (Fig. S3). Inhibitory inputs originate from interneurons that play an important regulatory role in brain development (Cossart, 2011) and migrate tangentially from the ganglionic eminence into the cortical plate to integrate into local circuits (Guo and Anton, 2014). Concurrently, Cdk5rap2 is highly expressed in the neocortex during neurogenesis and neuronal differentiation (Issa et al., 2013a), but present at lower levels during synaptogenesis that completes around P21. Loss of Cdk5rap2 prematurely shifts symmetric to asymmetric cell division leading to the earlier generation of postmitotic neurons (Buchman et al., 2010). This might impair the proper integration of interneurons into neocortical circuits on a spatio-temporal level and lead to increased interneuron death (Tuncdemir et al., 2016). Our results pointing to an impaired inhibition fit to the actual view on the importance of interneurons during neocortical development. Interneurons are critical for the integration and transmission of incoming synaptic inputs that drive maturation (Kilb, 2012), since functional GABAergic connections regulate network connectivity and excitation of pyramidal neurons (Isaacson and Scanziani, 2011). At early stages of cortical development, *i.e.* when neurons assume their positions and begin to mature, GABAergic inputs are required for the proper development of dendritic arbors and excitatory synaptic inputs (Maric et al., 2001; Wang and Kriegstein, 2008; Wang and Kriegstein, 2009). Aberrant synaptic connections may lead to excessive dendritic pruning contributing to the observed simplified dendritic arbor. Thus, our findings of reduced dendritic complexity and reduced inhibition are in line with these previous reports.

Maturation of inhibitory synaptic contacts on the soma of somatosensory neurons, in turn, depends on proper circuit function because it is impaired upon deficits in early activity or sensory experience (Chattopadhyaya et al., 2004; Jiao et al., 2006; Xue et al., 2014). Notably, in a previous study on adult neocortical layer 2/3 pyramidal neurons (Schuster et al., 2015) we did not detect an increase in EPSC frequency after blocking inhibition. This supports the view that during early synaptogenesis in (wild-type) mice GABA release results in more ambient GABA and suggests that this developmental regulation is impaired in *an/an* mice. Since cortical processing relies on the fine-tuned interplay between excitation and inhibition, healthy brains exhibit a tight control of E/I ratio in all cortical areas even after perturbations (House et al., 2011; Xue et al., 2014). This control is usually ensured by

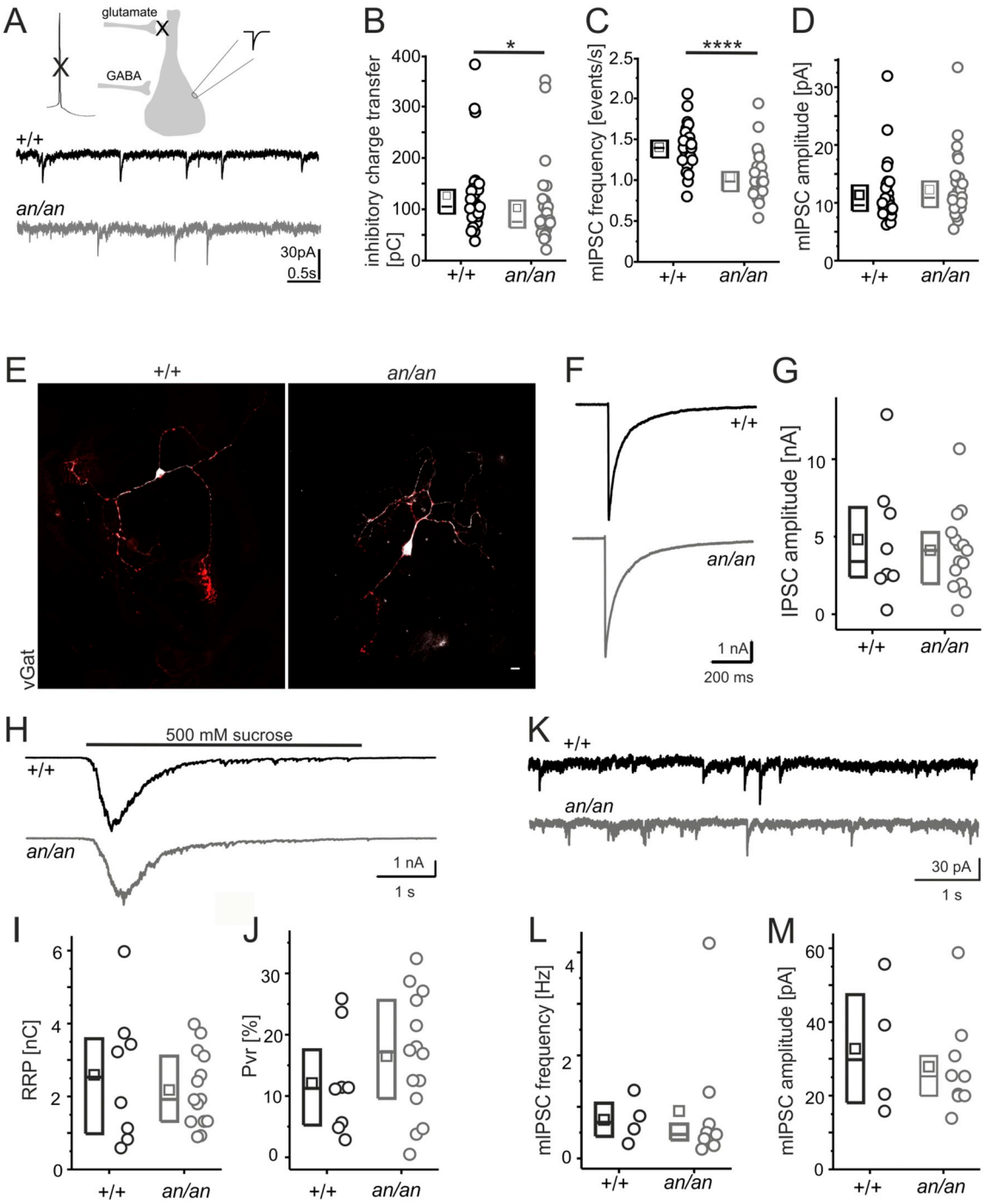

Fig. 6. Decreased inhibition at the soma of layer 2/3 neocortical *ex-vivo* pyramidal neurons in P6/7 but not in cultured neurons from *an/an* mice. (A) Scheme and example of mIPSCs traces recorded at −60 mV using equimolar Cl^- and blocking excitatory postsynaptic currents with CNQX and DAP-5 (n = 30 +/+ and 32 *an/an* neurons from 3 animals/group). (B and C) Box plots showing a decreased total inhibitory charge transfer in *an/an* mice (B) due to reduced mIPSCs frequency in *an/an* neurons (C). (D) Box plot graph depicting the mean mIPSC amplitudes shows no alteration between neurons from +/+ and *an/an* mice. Note that the slight reduction in serial resistance of *an/an* cells ($R_{s+/+}$ = 11.6 ± 0.7 MΩ *vs.* $R_{san/an}$ = 9.3 ± 0.6 MΩ, p = .009; not shown) might attenuate the difference in frequencies between the groups. (E) Photomicrographs of autaptic inhibitory neurons stained for Map2 (white) and VGat (red), scale bar: 10 µm. (F) Traces of inhibitory postsynaptic currents evoked by a 2 ms depolarization (IPSC). (G) Population data of evoked IPSC amplitudes from +/+ (black) and *an/an* (grey) autaptic cortical neurons. (H) Responses from +/+ (black) and *an/an* (grey) cortical neurons during 5 s application of 500 mM sucrose. (I) Box plot of readily releasable pool (RRP) and (J) average vesicular release probability (P_{vr} = IPSC charge / RRP charge) in autaptic +/+ and *an/an* neurons. (K) Traces of mIPSCs from +/+ (black) and *an/an* (grey) neurons. (L and M) Box plots of mIPSC frequencies (L) and mEPSC amplitudes (M). Data was collected from 2 independent cultures. (For interpretation of the references to colour in this figure legend, the reader is referred to the web version of this article.)

several regulators of E/I adjustment (House et al., 2011; Lin et al., 2008; Rico and Marín, 2011; Xue et al., 2014). Our results in *Cdk5rap2* mutants argue for an impaired E/I set point regulation as putatively caused by improper expression or targeting of molecules that control synaptic specificity. In line, our results of reduced number of inhibitory contacts while excitatory synapses and EPSC frequency was increased in *an/an* are mimicked when PSD95 amount was increased experimentally (Prange et al., 2004). Alternatively, inhibitory synaptogenesis

might be regulated without E/I balance compensation as shown for Npas4 (Lin et al., 2008).

Transient networks involve specific types of interneurons in deep and superficial layers of the neocortex (Lim et al., 2018) and the 2 most prevalent early born interneuron populations are SST^+ and PV^+, both generated in the MGE (Rudy et al., 2011). Since PV^+ neurons largely synapse on the soma of pyramidal neurons (Buhl et al., 1994) and are easy to recruit (Lazarus and Huang, 2011) they might represent a major source of early mIPSCs (Soltesz et al., 1995). PV^+ neurons that do not fulfill their inhibitory role might contribute to cognitive deficits (Marín, 2012) due to perturbed perisomatic and axo-axonic inhibition. This might lead to impaired oscillatory activity in the γ-frequency range (30–80 Hz, (Draguhn and Buzsáki, 2004), disturbed perisomatic feed-forward inhibition and therewith-reduced temporal precision of signal

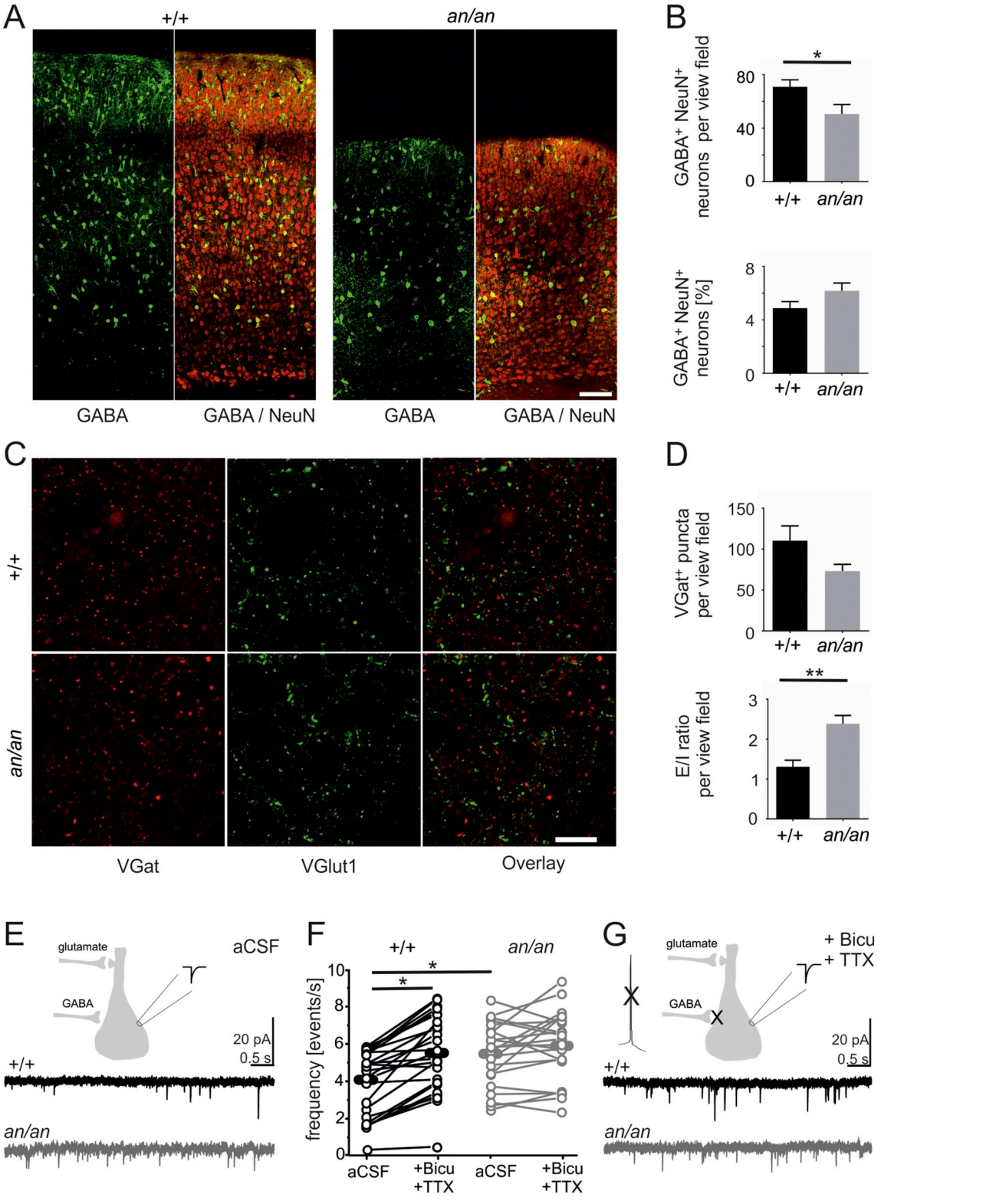

(caption on next page)

Fig. 7. Loss of GABAergic input adjusts excitatory drive in neocortical layer 2/3 pyramidal neurons of +/+ and *an/an* animals. (A) Coronal brain sections of P6-7 littermate animals stained for the interneuron/astrocyte marker GABA (green) and the neuronal marker NeuN (red) (immunofluorescence images, scale bar 100 μm). (B) The total number $GABA^+$ cells per view-field is reduced in *an/an* mice but the proportion of these cells in relation to total $NeuN^+$ neurons per view-field is comparable to +/+ mice. Note that there is no overlap of GABA and GFAP (Fig. S4), rendering an astrocytic contribution to $GABA^+$ cells unlikely. (C) Images of layer 2/3 areas (0.002 mm^2) of parietal cortices from littermate animals stained for VGlut1 (excitatory-presynaptic) and VGat (inhibitory-presynaptic) markers (confocal images, scale bar 10 μm). (D) The trend towards reduced number of inhibitory synapses contributes to an increased E/I ratio at layer 2/3 areas in *an/an* mice $n = 15$ images from 6 +/+ animals and 20 images from 6 *an/an* animals). (E and G) Comparative example of mEPSCs recorded at -60 mV before (E) and after blocking spontaneous action potentials and $GABA_A$ receptors with tetrodotoxin and bicuculline (+Bicu +TTX) (G) in +/+ (*black*) and *an/an* (*grey*) neurons. (F) Line series plots of PSC frequencies before (*aCSF*) and after blocking spontaneous action potentials and GABAergic transmission (+*Bicu* + *TTX*). In neurons from +/+ mice the EPSC frequency increased, whereas EPSC frequency remained comparable in *an/an*. Note that this differential effect led to similar total excitatory charge transfer (not shown) and mEPSCs frequency. The average amplitude was similar in +/+ and *an/an* pyramidal neurons (n = 30 +/+ and 26 *an/an* neurons from 4 animals/group). The serial resistance was comparable ($R_{s+/+} = 12.2 \pm 0.8$ MΩ *vs.* $R_{san/an} = 11.5 \pm 0.8$ MΩ, $p = .8$, MWU; not shown). (For interpretation of the references to colour in this figure legend, the reader is referred to the web version of this article.)

transduction in pyramidal neurons (Pouille and Scanziani, 2001) and misguided activity flow in local circuits (Xiang et al., 1998). However, synapses of PV^+ neurons (on pyramidal neurons and between PV^+) appear only at the end of the first postnatal week (Pangratz-Fuehrer and Hestrin, 2011) and might therefore contribute marginally to the observed effects. For the GABAergic synapses that are present before that (Luhmann and Prince, 1991), SST^+ provide a putative source (Takesian and Hensch, 2013). The loss or disturbance of SST^+ may cause dysfunctional early transient networks and therewith impair the maturation of other interneurons as PV^+ basket cells (Tuncdemir et al., 2016). It is also conceivable that a SST^+ neuronal loss / dysfunction would lead to disturbed oscillatory activity in the β-frequency range (15–30 Hz, (Draguhn and Buzsáki, 2004)).

Regardless of the cellular source, GABA reduction in the extracellular space might influence neuronal development by impairing: (a) neuronal migration in the embryonic cortex (López Bendito et al., 2003), (b) settlement of interneurons in the cortical plate (Bortone and Polleux, 2009), (c) formation of inhibitiory synapses (Oh et al., 2016) therewith setting the balance between inhibitory and excitatory synapses in early postnatal stages as foundation of later circuit development (Flores et al., 2015) and the neurogenesis of pyramidal neurons (Silva et al., 2018).

Interpreting the functional role of increased excitatory synapses is not that straightforward, given the lack of differences in excitatory drive after blocking inhibition (Fig. 7). If surplus excitatory synapses are on pyramidal neurons, they might be immature and silent. If they are on interneurons, they might represent an insufficient homoeostatic mechanism to increase inhibitory drive. In general, PV^+ neurons receive strong excitatory input from pyramidal neurons across and within layers and excitatory synapse number is modulated during development (Chung et al., 2017). This modulation might influence the maturation of working memory function since PV^+ neurons are key intermediates in a disinhibitory circuit motif for associative learning (Kepecs and Fishell, 2014).

Together, our results indicate that Cdk5rap2 influences E/I balance, dendrite arborization and spine morphogenesis in layer 2/3 neocortical pyramidal neurons further highlighting a connection between centrosomal biology and dendritic morphogenesis. These data are in line with the clinical finding that some MCPH patients suffer from hyperactivity and seizures. Since small dysregulations in E/I balance of cortical circuits, in particular due to developmental disruptions of interneuron integration (Bartolini et al., 2013), can have dramatic effects on entire cortical integration associated with the pathophysiology of neuropsychiatric (eminently in developmental) diseases (Nelson and Valakh, 2015), further studies in humans are warranted to analyze the significance of these findings for individuals with MCPH gene mutations.

4. Material and methods

4.1. Mice

All mouse experiments were carried out in accordance to state of Berlin rules (registration no. T0309/09). *Cdk5rap2* mutant or *Hertwig's anemia* mice (*an/an*) carrying an inversion of exon 4 (leading to exon skipping; (Lizarraga et al., 2010)) were generated by crossing heterozygous (+/*an*) mice (*C57BL/6* background; Jackson lab, stock no. 002306). Only 9.5% of the offspring carried a homozygous mutant genotype (*an/an*) at birth due to *in utero* lethality (Zaqout et al., 2017a). Most mutants die around postnatal day (P)7. Rare *an/an* mice surviving longer were also used for morphological studies ($n = 7$) and electrophysiological recordings ($n = 5$; P30–80). Neurons were regarded as mature (Z.-W. Zhang, 2004) and none of the parameters was correlated to age (table S2). The breeding was performed during the day, the day of birth was designated as P0. Genotyping was confirmed by PCR primers for (+/+) F 5′-TC ACT GAG CTG AAG AAG GAG AA-3′, R 5′-TGT CTT TCT GCC CTG ACA GT-3′ and (*an/an*) F 5′-GC AAT CAC TAA AAT GTC CGA TT-3′, R 5′-TGT CTT TCT GCC CTG ACA GT-3′.

4.2. Nissl staining and neocortical dimension analysis

After dissection, brains were fixed in 4% PFA for overnight, dehydrated in an ethanol series (50, 70, 85, 90, 100%), cleaned with xylene, and embedded in paraffin. 10 μm sections were cut on a microtome and collected on Superfrost plus slides®. De-paraffinized coronal brain sections at the level of corpus callosum and anterior commissure were incubated in 1% cresyl violet (C5042, Sigma-Aldrich, USA) in acetate-buffered solution (pH 4.5) for 5 min. At the level of corpus callosum and anterior commissure, parietal cortical thickness was measured perpendicularly to pial surface, and neocortical area was estimated using ImageJ software.

4.3. Golgi staining, dendritic complexity, and spine analysis

Golgi-Cox impregnation of adult brain samples was performed as described (Zaqout and Kaindl, 2016). Briefly, brains were immersed in the impregnation solution in darkness at room temperature (RT) for 2 weeks, and transferred into tissue-protectant solution at 4 °C for 4 days. Brains were cut into 200 μm sections for dendritic complexity analysis and 100 μm sections for dendritic spine analysis as described previously (Schuster et al., 2015). Sections were collected on gelatin-coated slides, left to dry for 2 days, developed, dehydrated through ethanol series, cleared in xylol solution, and mounted in Eukitt (quick-252 hardening mounting medium; 03989, Fluka analytical, Germany). For dendritic complexity assessment, Sholl analysis (Sholl, 1953) was performed for layer 2/3 pyramidal neurons of matched +/+ and *an/an*

somatosensory neocortical regions. The total intersection number of the dendritic tree with 30 10-μm spaced concentric circles were counted with cell counter plug-ins in ImageJ. Neurite tracer plug-in in Fiji/ImageJ was used to draw representative neurons. The number of spines was counted in 20 μm long segments of secondary basal dendrites using ImageJ. Spines were classified to one of three morphological subtypes: mushroom (short neck, large bulbous end), stubby (no neck) and thin-shaped (long neck).

4.4. Immunohistology and immunocytology

Paraffin sections were deparaffinized, exposed to heat-mediated antigen retrieval citrate-based solution (pH 6.0; H-3300, Vector Laboratories, USA), blocked for 1 h with 10% donkey or goat normal serum at RT, and incubated overnight with the primary antibody at RT followed by an incubation with the corresponding secondary antibodies for 2 h at RT. The following primary antibodies were used at specified dilutions: rabbit anti-Cux1 (1:200; Santa Cruz Biotechnology, Heidelberg, Germany, sc-13,024 (Issa et al., 2013a)), rat anti-Ctip2 (1:250; Abcam, Cambridge, UK, ab18465 (Issa et al., 2013a)), mouse anti-GABA (GABA, 1:100; Chemicon, Temecula CA, MAB316 (Uematsu et al., 2008)), rabbit anti-NeuN (1:200; Merck-Millipore, Germany, ABN78 (Issa et al., 2013a)), guinea pig anti-vesicular glutamate transporter 1 (VGlut1, 1:500; Merck-Millipore, Germany, AB5905 (Mitchell et al., 2012)), rabbit anti-vesicular GABA transporter (VGat, 1:500; Merck-Millipore, Germany, AB5062P (Mitchell et al., 2012)), and rabbit anti-post synaptic density 95 (PSD95, 1:200; Synaptic System, Göttingen, Germany, 124-002 (Schuster et al., 2015)). Secondary antibodies were used at 1:400 dilution: donkey Cy3-conjugated anti-rabbit and anti-mouse IgG (Jackson ImmunoResearch, Suffolk, UK), donkey Alexa Fluor® 488 conjugate anti-rat, and anti-guinea pig IgG (Invitrogen, Darmstadt, Germany). Nuclei were stained with 40,6-diamidino-2-phenylindole (DAPI, 1:1000, Sigma-Aldrich, USA). Neuronal cultures were prepared from cortices of P0 – P2 +/+ and *an/an* mice and stained with vesicular glutamate transporter 1 (VGlut1; excitatory presynaptic marker; green) or vesicular GABA transporter (VGat; inhibitory presynaptic marker; red). Staining of microtubule network with microtubule-associated protein Map2a (white) was used to display soma and dendritic tree of individual neurons and count the number of cells per view field. Cultures were fixed at DIV 14–16 with 4% PFA for 10 min and permeabilized with 1xPBS + 0.1% Tween 20 (PBS-T). Cells were blocked with PBS-T containing 5% donkey serum for 1 h, before applying the primary antibody overnight at 4 °C (anti-Map2a, Millipore, anti-VGlut1 and anti-VGat, Synaptic Systems). The secondary fluorophore-conjugated antibody was incubated for 1 h at RT. All antibodies used in this paper are well established and were previously applied by others and us on mouse tissue. In addition, negative control staining experiments including the application of the secondary antibody only have been performed (Fig. S1).

4.5. Electrophysiology on ex-vivo brain slices

Slices of mouse brains (P6/7 and adult) were used for *ex-vivo* recordings. Mice were decapitated, brains removed, and transferred to ice-cold artificial cerebrospinal fluid (ACSF) containing in mM 85 NaCl, 26 $NaHCO_3$, 2.5 KCl, 1 NaH_2PO_4, 0.5 $CaCl_2$, 7 $MgCl_2$, 50 sucrose, and 10 glucose (290–310 mOsm). Coronal slices (300 μm thick) containing somatosensory cortex were cut on a Leica VT1200S (Leica Microsystems, Germany). Slices recovered for 30 min at 34 °C and were kept at room temperature afterwards. Somatic whole-cell recordings were performed in a submerged recording chamber perfused with ACSF containing in mM 117 NaCl, 3.5 KCl, 1.25 NaH_2PO4, 2 $MgSO_4$ or $MgCl_2$, 26 NaHCO3, 10 glucose, and 2 $CaCl_2$. All ACSF solutions were constantly gassed with 95% O_2/5% CO_2, osmolarity was between 290 and 305 mosmol/l, and experiments were performed at 32–34 °C. Pyramidal neurons were visually identified in layer 2/3 using an upright microscope equipped with infrared differential interference contrast optics (Axioskop FS2; Zeiss or Olympus BX51, Germany). Whole-cell patch clamp recordings were conducted with pipettes (tip resistance 3–5 MΩ) filled with intracellular solution containing in mM 120 K-gluconate, 10 KCl, 10 Na-phosphocreatine, 1 $MgCl_2$, 1 $CaCl_2$, 11 EGTA, 10 HEPES, 2 Mg -ATP, 0.3 Tris-GTP (pH 7.25, 288 mOsm). Only neurons with resting potentials below −65 mV and spiking characteristics of pyramidal neurons were included in the analysis. Input resistance was calculated with a linear fit of the current clamp generated I-V plot in close vicinity of the resting potential. Intersection of the linear regression of the F-I relationship (estimated in the linear range) and abscissa roughly approximated the rheobase. Postsynaptic currents were recorded in voltage clamp at a holding potential of −60 mV. Under these conditions, most spontaneous postsynaptic events are mediated by activation of glutamatergic, AMPA receptor mediated currents (Schuster et al., 2015). Miniature postsynaptic currents (mPSCs) were recorded in the presence of 0.5–1 μM tetrodotoxin (TTX). mEPSCs were analyzed in presence of bicuculline (20 μM) while mIPSC were analyzed in presence of 10 μM CNQX and 25 μM D-AP5 and with KCl-based internal solutions (all Tocris Bioscience). Data from patch-clamp recordings were collected with an EPC-10 double amplifier (HEKA, Germany), digitized (10 kHz, after Bessel filtering at 2.9 kHz), and stored using PatchMaster software (HEKA). Series resistance (R_S) was monitored throughout experiments; neurons were rejected if R_S was > 20 MΩ or varied > ± 30%. No R_S compensation was used. Liquid junction potentials were not corrected for. Synaptic events were detected offline using the Mini Analysis Program (Synaptosoft Inc., USA) and a threshold of 3.5 times noise (standard deviation of regions without manually detectable postsynaptic currents). All events were visually counterchecked. As integrated measure the total charge transfer was calculated from the equation: $Q = f \times Q_{PSCs}$, where f is the frequency (s^{-1}), and Q_{PSCs} is the average charge transfer for each PSC (Ataka and Gu, 2006). Paired EPSCs (50 ms interval) were elicited by square pulse (100 μs) stimulation of the slice 50–100 μm lateral of the recording electrode at the border between layer 2/3 and 4 with a concentric tungsten electrode (TM33CCINS, WPI, USA). All compounds used were purchased from Sigma-Aldrich, Germany unless stated otherwise.

4.6. Electrophysiology on dissociated cell cultures

Autaptic and continental primary neuronal cultures were prepared from the cortices of newborn (P0-P2) mice, and neurons were plated on astrocyte feeder layer from cortices of non-mutated *C57/Bl6* mouse pups (P0-P2; prepared 2 weeks before plating the neurons) as previously described (Wu et al., 2015). Briefly, cortices were removed, enzymatically and mechanically dissociated. Neurons were cultured in Neurobasal-A media containing B-27 Supplement, 10 IU/ml penicillin, 1 g/ml streptomycin, and 2 mM L-alanyl-L-glutamine. The seeding density for continental cultures was 1.35×10^4 cells/cm^2. Cultures with different genotypes were generated from siblings that were treated identically during culturing and incubated at 37 °C with 5% CO_2. Whole cell voltage-clamp recordings from autaptic cortical neurons were obtained between *days in vitro* (DIV) 14–16 at RT. Recordings and analysis of data were done as previously described (Wu et al., 2015). Extracellular solution contained in mM: 140 NaCl, 2.4 KCl, 10 HEPES, 10 glucose, 2 $CaCl_2$, and 4 $MgCl_2$. The pipette internal solution contained in mM: 136 KCl, 17.8 HEPES, 1 EGTA, 4.6 $MgCl_2$, 4 ATP-Na_2, 0.3 GTP-Na_2, 12 creatine phosphate, and 50 U/ml phosphocreatine kinase. Both extracellular and internal solutions were adjusted to pH 7.4 and osmolarity of ~300 mOsm. Borosilicate glass pipettes had a resistance of 3–4 MΩ. Recordings were performed with a MultiClamp 700B amplifier, and data were acquired with Clampex 10.0 (Molecular Devices). To verify glutamatergic responses in autaptic cultures, 3 mM kynurenic acid was applied to the extracellular solution. Sucrose solution (500 mM added to external solution) was applied for 5 s to assess the

size of the readily releasable pool (RRP; (Rosenmund and Stevens, 1996)). Evoked EPSCs were recorded after somatic depolarization from −70 to 0 mV for 2 ms. Vesicular release probability (*Pvr*) was determined by calculating the EPSC charge divided by the RRP charge of individual neurons. Spontaneous release was determined as mEPSC and was recorded for 60 s at −70 mV. To subtract background noise, recording was performed with the application of 3 mM kynurenic acid for the same duration. Traces were filtered at 1 kHz, and events were detected by using a template-based algorithm in AxoGraphX. Data was collected from two independent cultures.

4.7. Imaging

Brightfield images of Nissl-stained brain sections and Golgi-stained dendritic spines were taken by Olympus BX60 microscope equipped with an Axiocam MRc Zeiss camera and Axiovision 4.8 software (Zeiss, Göttingen, Germany). For studying dendritic arborization, 1-µm-spaced *Z*-stack brightfield images were taken by an Olympus IX81 microscope equipped with an F View II (sw) camera (Soft Imaging System GmbH, Münster, Germany). Fluorescent images of layer markers were taken by Olympus BX51 microscope by an Intas camera and Magnafire 2.1B software (Olympus, Hamburg, Germany). Fluorescent images of synaptic markers were taken by an lsm5exciter Zeiss confocal microscope with the software Zen (version 2009, Zeiss, Jena, Germany). Fluorescent images of dissociated cell culture were taken with an Olympus IX81 epifluorescent microscope. All images were processed using Adobe Photoshop CS6 version 13.0 × 64 and Fiji/ImageJ software.

4.8. Statistical analysis

For *in-vivo* parietal cortical thickness, neocortical area, cortical layers, Scholl analysis, and spine density statistics, two-tailed Student's *t*-tests (TT) were applied. Statistics of *ex-vivo* brain slices electrophysiology were performed using Origin8.5 (OriginLab, USA). For normally distributed datasets (Shapiro-Wilk test) TT was used. In the case of significant deviations from normal distribution ($p \leq .05$) the non-parametric Mann-Whitney-*U* test (MWU) was used. The frequency of mEPSCs before and after application of bicuculline was analyzed with two way repeated measures ANOVA and *post hoc* Bonferroni multiple-comparison tests (ANOVA-RM-B). Data of dissociated cell cultures were first tested for a Gaussian distribution with D'Agostino and Pearson omnibus normality test. If data were normally distributed, one-way ANOVA followed by Bonferroni multiple-comparison tests were performed. Otherwise, nonparametric Kruskal-Wallis test followed by Dunn multiple comparison tests were used.

Supplementary data to this article can be found online at https://doi.org/10.1016/j.nbd.2019.05.008.

Authors' contributions

AMK, US, and CR were responsible for project conception. AMK, SZ, KB and US wrote the manuscript. SZ, KB, YJW, SO, US, LLB, MR and NK performed and analyzed the experiments. All authors read, revised, and approved the final manuscript.

Acknowledgments

The authors thank Victor Tarabykin, Imre Vida, Paraskevi Bessa, Pina Knauff, Jutta Schüler, Gisela Stoltenburg, Jessica Fassbender, Susanne Kosanke, Magdalena John, Julia König and Claudia Pallasch for discussions and/or technical assistance as well as Janna Lehnhoff and Noah L. Döhne for conducting some of the patch clamp experiments. The German Research Foundation (DFG, SFB665, SFB1315), the Helmholtz Association the Berlin Institute of Health (BIH), the German Academic Exchange Service (DAAD), and the Charité – Universitätsmedizin Berlin, supported this work.

Conflicts of interest

The authors declare that they have no competing interests.

References

Ataka, T., Gu, J.G., 2006. Relationship between tonic inhibitory currents and phasic inhibitory activity in the spinal cord lamina II region of adult mice. Mol. Pain 2, 36. https://doi.org/10.1186/1744-8069-2-36.

Barrera, J.A., Kao, L.-R., Hammer, R.E., Seemann, J., Fuchs, J.L., Megraw, T.L., 2010. CDK5RAP2 regulates centriole engagement and cohesion in mice. Dev. Cell 18, 913–926. https://doi.org/10.1016/j.devcel.2010.05.017.

Bartolini, G., Ciceri, G., Marín, O., 2013. Integration of GABAergic interneurons into cortical cell assemblies: lessons from embryos and adults. Neuron 79, 849–864. https://doi.org/10.1016/j.neuron.2013.08.014.

Bond, J., Roberts, E., Springell, K., Lizarraga, S.B., Lizarraga, S., Scott, S., Higgins, J., Hampshire, D.J., Morrison, E.E., Leal, G.F., Silva, E.O., Costa, S.M.R., Baralle, D., Raponi, M., Karbani, G., Rashid, Y., Jafri, H., Bennett, C., Corry, P., Walsh, C.A., Woods, C.G., 2005. A centrosomal mechanism involving CDK5RAP2 and CENPJ controls brain size. Nat. Genet. 37, 353–355. https://doi.org/10.1038/ng1539.

Bortone, D., Polleux, F., 2009. KCC2 expression promotes the termination of cortical interneuron migration in a voltage-sensitive calcium-dependent manner. Neuron 62, 53–71. https://doi.org/10.1016/j.neuron.2009.01.034.

Buchman, J.J., Tseng, H.-C., Zhou, Y., Frank, C.L., Xie, Z., Tsai, L.-H., 2010. Cdk5rap2 interacts with pericentrin to maintain the neural progenitor pool in the developing neocortex. Neuron 66, 386–402. https://doi.org/10.1016/j.neuron.2010.03.036.

Buhl, E.H., Halasy, K., Somogyi, P., 1994. Diverse sources of hippocampal unitary inhibitory postsynaptic potentials and the number of synaptic release sites. Nature 368, 823–828. https://doi.org/10.1038/368823a0.

Chattopadhyaya, B., Di Cristo, G., Higashiyama, H., Knott, G.W., Kuhlman, S.J., Welker, E., Huang, Z.J., 2004. Experience and activity-dependent maturation of perisomatic GABAergic innervation in primary visual cortex during a postnatal critical period. J. Neurosci. 24, 9598–9611. https://doi.org/10.1523/JNEUROSCI.1851-04.2004.

Chung, D.W., Wills, Z.P., Fish, K.N., Lewis, D.A., 2017. Developmental pruning of excitatory synaptic inputs to parvalbumin interneurons in monkey prefrontal cortex. Proc. Natl. Acad. Sci. U. S. A. 114, E629–E637. https://doi.org/10.1073/pnas.1610077114.

Cossart, R., 2011. The maturation of cortical interneuron diversity: how multiple developmental journeys shape the emergence of proper network function. Curr. Opin. Neurobiol. 21, 160–168. https://doi.org/10.1016/j.conb.2010.10.003.

Dailey, M.E., Smith, S.J., 1996. The dynamics of dendritic structure in developing hippocampal slices. J. Neurosci. 16, 2983–2994.

del Castillo, J., Katz, B., 1954. Quantal components of the end-plate potential. J. Physiol. 124, 560–573.

DiStasio, A., Driver, A., Sund, K., Donlin, M., Muraleedharan, R.M., Pooya, S., Kline-Fath, B., Kaufman, K.M., Prows, C.A., Schorry, E., Dasgupta, B., Stottmann, R.W., 2017. Copb2 is essential for embryogenesis and hypomorphic mutations cause human microcephaly. Hum. Mol. Genet. 26, 4836–4848. https://doi.org/10.1093/hmg/ddx362.

Draguhn, A., Buzsáki, G., 2004. Neuronal oscillations in cortical networks. Science 304, 1926–1929. https://doi.org/10.1126/science.1099745.

Fish, J.L., Kosodo, Y., Enard, W., Pääbo, S., Huttner, W.B., 2006. Aspm specifically maintains symmetric proliferative divisions of neuroepithelial cells. Proc. Natl. Acad. Sci. U. S. A. 103, 10438–10443. https://doi.org/10.1073/pnas.0604066103.

Flores, C.E., Nikonenko, I., Mendez, P., Fritschy, J.-M., Tyagarajan, S.K., Muller, D., 2015. Activity-dependent inhibitory synapse remodeling through gephyrin phosphorylation. Proc. Natl. Acad. Sci. U. S. A. 112, E65–E72. https://doi.org/10.1073/pnas.1411170112.

Fong, K.-W., Choi, Y.-K., Rattner, J.B., Qi, R.Z., 2008. CDK5RAP2 is a pericentriolar protein that functions in centrosomal attachment of the gamma-tubulin ring complex. Mol. Biol. Cell 19, 115–125. https://doi.org/10.1091/mbc.E07-04-0371.

Guo, J., Anton, E.S., 2014. Decision making during interneuron migration in the developing cerebral cortex. Trends Cell Biol. 24, 342–351. https://doi.org/10.1016/j.tcb.2013.12.001.

Hassan, M.J., Khurshid, M., Azeem, Z., John, P., Ali, G., Chishti, M.S., Ahmad, W., 2007. Previously described sequence variant in CDK5RAP2 gene in a Pakistani family with autosomal recessive primary microcephaly. BMC Med. Genet. 8, 58. https://doi.org/10.1186/1471-2350-8-58.

House, D.R.C., Elstrott, J., Koh, E., Chung, J., Feldman, D.E., 2011. Parallel regulation of feedforward inhibition and excitation during whisker map plasticity. Neuron 72, 819–831. https://doi.org/10.1016/j.neuron.2011.09.008.

Isaacson, J.S., Scanziani, M., 2011. How inhibition shapes cortical activity. Neuron 72, 231–243. https://doi.org/10.1016/j.neuron.2011.09.027.

Issa, L., Kraemer, N., Rickert, C.H., Sifringer, M., Ninnemann, O., Stoltenburg-Didinger, G., Kaindl, A.M., 2013a. CDK5RAP2 expression during murine and human brain development correlates with pathology in primary autosomal recessive microcephaly.

Cereb. Cortex 23, 2245–2260. https://doi.org/10.1093/cercor/bhs212.
Issa, L., Mueller, K., Seufert, K., Kraemer, N., Rosenkotter, H., Ninnemann, O., Buob, M., Kaindl, A.M., Morris-Rosendahl, D.J., 2013b. Clinical and cellular features in patients with primary autosomal recessive microcephaly and a novel CDK5RAP2 mutation. Orphanet. J. Rare Dis. 8, 59. https://doi.org/10.1186/1750-1172-8-59.
Jiao, Y., Zhang, C., Yanagawa, Y., Sun, Q.-Q., 2006. Major effects of sensory experiences on the neocortical inhibitory circuits. J. Neurosci. 26, 8691–8701. https://doi.org/10.1523/JNEUROSCI.2478-06.2006.
Kadir, R., Harel, T., Markus, B., Perez, Y., Bakhrat, A., Cohen, I., Volodarsky, M., Feintsein-Linial, M., Chervinski, E., Zlotogora, J., Sivan, S., Birnbaum, R.Y., Abdu, U., Shalev, S., Birk, O.S., 2016. ALFY-controlled DVL3 autophagy regulates Wnt signaling, determining human brain size. PLoS Genet. 12, e1005919. https://doi.org/10.1371/journal.pgen.1005919.
Kaindl, A.M., Passemard, S., Kumar, P., Kraemer, N., Issa, L., Zwirner, A., Gerard, B., Verloes, A., Mani, S., Gressens, P., 2010. Many roads lead to primary autosomal recessive microcephaly. Prog. Neurobiol. 90, 363–383. https://doi.org/10.1016/j.pneurobio.2009.11.002.
Kepecs, A., Fishell, G., 2014. Interneuron cell types are fit to function. Nature 505, 318–326. https://doi.org/10.1038/nature12983.
Kilb, W., 2012. Development of the GABAergic system from birth to adolescence. Neuroscientist 18, 613–630. https://doi.org/10.1177/1073858411422114.
Kim, A.H., Puram, S.V., Bilimoria, P.M., Ikeuchi, Y., Keough, S., Wong, M., Rowitch, D., Bonni, A., 2009. A centrosomal Cdc20-APC pathway controls dendrite morphogenesis in postmitotic neurons. Cell 136, 322–336. https://doi.org/10.1016/j.cell.2008.11.050.
Kraemer, N., Issa, L., Hauck, S.C.R., Mani, S., Ninnemann, O., Kaindl, A.M., 2011. What's the hype about CDK5RAP2? Cell. Mol. Life Sci. 68, 1719–1736. https://doi.org/10.1007/s00018-011-0635-4.
Kraemer, N., Ravindran, E., Zaqout, S., Neubert, G., Schindler, D., Ninnemann, O., Gräf, R., Seiler, A.E.M., Kaindl, A.M., 2015. Loss of CDK5RAP2 affects neural but not non-neural mESC differentiation into cardiomyocytes. Cell Cycle 14, 2044–2057. https://doi.org/10.1080/15384101.2015.1044169.
Lazarus, M.S., Huang, Z.J., 2011. Distinct maturation profiles of perisomatic and dendritic targeting GABAergic interneurons in the mouse primary visual cortex during the critical period of ocular dominance plasticity. J. Neurophysiol. 106, 775–787. https://doi.org/10.1152/jn.00729.2010.
Lim, L., Mi, D., Llorca, A., Marín, O., 2018. Development and functional diversification of cortical interneurons. Neuron 100, 294–313. https://doi.org/10.1016/j.neuron.2018.10.009.
Lin, Y., Bloodgood, B.L., Hauser, J.L., Lapan, A.D., Koon, A.C., Kim, T.-K., Hu, L.S., Malik, A.N., Greenberg, M.E., 2008. Activity-dependent regulation of inhibitory synapse development by Npas4. Nature 455, 1198–1204. https://doi.org/10.1038/nature07319.
Lizarraga, S.B., Margossian, S.P., Harris, M.H., Campagna, D.R., Han, A.-P., Blevins, S., Mudbhary, R., Barker, J.E., Walsh, C.A., Fleming, M.D., 2010. Cdk5rap2 regulates centrosome function and chromosome segregation in neuronal progenitors. Development 137, 1907–1917. https://doi.org/10.1242/dev.040410.
López Bendito, G., Luján, R., Shigemoto, R., Ganter, P., Paulsen, O., Molnár, Z., 2003. Blockade of GABA(B) receptors alters the tangential migration of cortical neurons. Cereb. Cortex 13, 932–942.
Luhmann, H.J., Prince, D.A., 1991. Postnatal maturation of the GABAergic system in rat neocortex. J. Neurophysiol. 65, 247–263. https://doi.org/10.1152/jn.1991.65.2.247.
Maric, D., Liu, Q.Y., Maric, I., Chaudry, S., Chang, Y.H., Smith, S.V., Sieghart, W., Fritschy, J.M., Barker, J.L., 2001. GABA expression dominates neuronal lineage progression in the embryonic rat neocortex and facilitates neurite outgrowth via GABA(A) autoreceptor/Cl- channels. J. Neurosci. 21, 2343–2360.
Marín, O., 2012. Interneuron Dysfunction in Psychiatric Disorders. vol. 13. Nature Publishing Group, pp. 107–120. https://doi.org/10.1038/nrn3155.
Matsuzaki, M., Ellis-Davies, G.C., Nemoto, T., Miyashita, Y., Iino, M., Kasai, H., 2001. Dendritic spine geometry is critical for AMPA receptor expression in hippocampal CA1 pyramidal neurons. Nat. Neurosci. 4, 1086–1092. https://doi.org/10.1038/nn736.
Mitchell, N., Petralia, R.S., Currier, D.G., Wang, Y.-X., Kim, A., Mattson, M.P., Yao, P.J., 2012. Sonic hedgehog regulates presynaptic terminal size, ultrastructure and function in hippocampal neurons. J. Cell Sci. 125, 4207–4213. https://doi.org/10.1242/jcs.105080.
Moawia, A., Shaheen, R., Rasool, S., Waseem, S.S., Ewida, N., Budde, B., Kawalia, A., Motameny, S., Khan, K., Fatima, A., Jameel, M., Ullah, F., Akram, T., Ali, Z., Abdullah, U., Irshad, S., Höhne, W., Noegel, A.A., Al-Owain, M., Hörtnagel, K., Stöbe, P., Baig, S.M., Nürnberg, P., Alkuraya, F.S., Hahn, A., Hussain, M.S., 2017. Mutations of KIF14 cause primary microcephaly by impairing cytokinesis. Ann. Neurol. 82, 562–577. https://doi.org/10.1002/ana.25044.
Nair, D., Hosy, E., Petersen, J.D., Constals, A., Giannone, G., Choquet, D., Sibarita, J.-B., 2013. Super-resolution imaging reveals that AMPA receptors inside synapses are dynamically organized in nanodomains regulated by PSD95. J. Neurosci. 33, 13204–13224. https://doi.org/10.1523/JNEUROSCI.2381-12.2013.
Nelson, S.B., Valakh, V., 2015. Excitatory/inhibitory balance and circuit homeostasis in autism spectrum disorders. Neuron 87, 684–698. https://doi.org/10.1016/j.neuron.2015.07.033.
Oh, W.C., Lutzu, S., Castillo, P.E., Kwon, H.-B., 2016. De novo synaptogenesis induced by GABA in the developing mouse cortex. Science 353, 1037–1040. https://doi.org/10.1126/science.aaf5206.
Pangratz-Fuehrer, S., Hestrin, S., 2011. Synaptogenesis of electrical and GABAergic synapses of fast-spiking inhibitory neurons in the neocortex. J. Neurosci. 31, 10767–10775. https://doi.org/10.1523/JNEUROSCI.6655-10.2011.
Passemard, S., Titomanlio, L., Elmaleh, M., Afenjar, A., Alessandri, J.-L., Andria, G., de Villemeur, T.B., Boespflug-Tanguy, O., Burglen, L., Del Giudice, E., Guimiot, F., Hyon, C., Isidor, B., Mégarbané, A., Moog, U., Odent, S., Hernandez, K., Pouvreau, N., Scala, I., Schaer, M., Gressens, P., Gerard, B., Verloes, A., 2009. Expanding the clinical and neuroradiologic phenotype of primary microcephaly due to ASPM mutations. Neurology 73, 962–969. https://doi.org/10.1212/WNL.0b013e3181b8799a.
Pouille, F., Scanziani, M., 2001. Enforcement of temporal fidelity in pyramidal cells by somatic feed-forward inhibition. Science 293, 1159–1163. https://doi.org/10.1126/science.1060342.
Prange, O., Wong, T.P., Gerrow, K., Wang, Y.T., El-Husseini, A., 2004. A balance between excitatory and inhibitory synapses is controlled by PSD-95 and neuroligin. Proc. Natl. Acad. Sci. U. S. A. 101, 13915–13920. https://doi.org/10.1073/pnas.0405939101.
Rico, B., Marín, O., 2011. Neuregulin signaling, cortical circuitry development and schizophrenia. Curr. Opin. Genet. Dev. 21, 262–270. https://doi.org/10.1016/j.gde.2010.12.010.
Rosenmund, C., Stevens, C.F., 1996. Definition of the readily releasable pool of vesicles at hippocampal synapses. Neuron 16, 1197–1207.
Rudy, B., Fishell, G., Lee, S., Hjerling-Leffler, J., 2011. Three groups of interneurons account for nearly 100% of neocortical GABAergic neurons. Dev. Neurobiol. 71, 45–61. https://doi.org/10.1002/dneu.20853.
Schuster, S., Rivalan, M., Strauss, U., Stoenica, L., Trimbuch, T., Rademacher, N., Parthasarathy, S., Lajkó, D., Rosenmund, C., Shoichet, S.A., Winter, Y., Tarabykin, V., Rosário, M., 2015. NOMA-GAP/ARHGAP33 regulates synapse development and autistic-like behavior in the mouse. Mol. Psychiatry 20, 1120–1131. https://doi.org/10.1038/mp.2015.42.
Sholl, D.A., 1953. Dendritic organization in the neurons of the visual and motor cortices of the cat. J. Anat. 87, 387–406.
Silva, C.G., Peyre, E., Adhikari, M.H., Tielens, S., Tanco, S., Van Damme, P., Magno, L., Krusy, N., Agirman, G., Magiera, M.M., Kessaris, N., Malgrange, B., Andrieux, A., Janke, C., Nguyen, L., 2018. Cell-intrinsic control of interneuron migration drives cortical morphogenesis. Cell 172, 1063–1078.e19. https://doi.org/10.1016/j.cell.2018.01.031.
Soltesz, I., Smetters, D.K., Mody, I., 1995. Tonic inhibition originates from synapses close to the soma. Neuron 14, 1273–1283.
Spruston, N., Jaffe, D.B., Williams, S.H., Johnston, D., 1993. Voltage- and space-clamp errors associated with the measurement of electrotonically remote synaptic events. J. Neurophysiol. 70, 781–802. https://doi.org/10.1152/jn.1993.70.2.781.
Takesian, A.E., Hensch, T.K., 2013. Balancing plasticity/stability across brain development. Prog. Brain Res. 207, 3–34. https://doi.org/10.1016/B978-0-444-63327-9.00001-1.
Tuncdemir, S.N., Wamsley, B., Stam, F.J., Osakada, F., Goulding, M., Callaway, E.M., Rudy, B., Fishell, G., 2016. Early somatostatin interneuron connectivity mediates the maturation of deep layer cortical circuits. Neuron 89, 521–535. https://doi.org/10.1016/j.neuron.2015.11.020.
Turrigiano, G., Leslie, K.R., Desai, N.S., Rutherford, L.C., Nelson, S.B., 1998. Activity-dependent scaling of quantal amplitude in neocortical neurons. Nature 391, 892–896. https://doi.org/10.1038/36103.
Uematsu, M., Hirai, Y., Karube, F., Ebihara, S., Kato, M., Abe, K., Obata, K., Yoshida, S., Hirabayashi, M., Yanagawa, Y., Kawaguchi, Y., 2008. Quantitative chemical composition of cortical GABAergic neurons revealed in transgenic venus-expressing rats. Cereb. Cortex 18, 315–330. https://doi.org/10.1093/cercor/bhm056.
Wang, D.D., Kriegstein, A.R., 2008. GABA regulates excitatory synapse formation in the neocortex via NMDA receptor activation. J. Neurosci. 28, 5547–5558. https://doi.org/10.1523/JNEUROSCI.5599-07.2008.
Wang, D.D., Kriegstein, A.R., 2009. Defining the role of GABA in cortical development. J. Physiol. 587, 1873–1879. https://doi.org/10.1113/jphysiol.2008.167635.
Wu, Y.-J., Tejero, R., Arancillo, M., Vardar, G., Korotkova, T., Kintscher, M., Schmitz, D., Ponomarenko, A., Tabares, L., Rosenmund, C., 2015. Syntaxin 1B is important for mouse postnatal survival and proper synaptic function at the mouse neuromuscular junctions. J. Neurophysiol. 114, 2404–2417. https://doi.org/10.1152/jn.00577.2015.
Xiang, Z., Huguenard, J.R., Prince, D.A., 1998. Cholinergic switching within neocortical inhibitory networks. Science 281, 985–988.
Xue, M., Atallah, B.V., Scanziani, M., 2014. Equalizing excitation-inhibition ratios across visual cortical neurons. Nature 511, 596–600. https://doi.org/10.1038/nature13321.
Yoon, B.-E., Lee, C.J., 2014. GABA as a rising gliotransmitter. Front. Neural. Circ. 8, 141. https://doi.org/10.3389/fncir.2014.00141.
Zaqout, S., Kaindl, A.M., 2016. Golgi-cox staining step by step. Front. Neuroanat. 10, 38. https://doi.org/10.3389/fnana.2016.00038.
Zaqout, S., Bessa, P., Krämer, N., Stoltenburg-Didinger, G., Kaindl, A.M., 2017a. CDK5RAP2 is required to maintain the germ cell pool during embryonic development. Stem Cell Rep. 8, 198–204. https://doi.org/10.1016/j.stemcr.2017.01.002.
Zaqout, S., Morris-Rosendahl, D., Kaindl, A.M., 2017b. Autosomal recessive primary microcephaly (MCPH): an update. Neuropediatrics 48, 135–142. https://doi.org/10.1055/s-0037-1601448.
Zhang, Z.-W., 2004. Maturation of layer V pyramidal neurons in the rat prefrontal cortex: intrinsic properties and synaptic function. J. Neurophysiol. 91, 1171–1182. https://doi.org/10.1152/jn.00855.2003.
Zhang, X., Liu, D., Lv, S., Wang, H., Zhong, X., Liu, B., Wang, B., Liao, J., Li, J., Pfeifer, G.P., Xu, X., 2009. CDK5RAP2 is required for spindle checkpoint function. Cell Cycle 8, 1206–1216. https://doi.org/10.4161/cc.8.8.8205.